Bacteria hijack a neuro-immune axis in the meninges to facilitate brain invasion

Isaac Chiu (isaac_chiu@hms.harvard.edu)
Harvard Medical School https://orcid.org/0000-0002-0723-4841

Felipe Pinho-Ribeiro
Harvard Medical School

Liwen Deng
Department of Immunology, Blavatnik Institute, Harvard Medical School

Dylan Neel
Harvard Medical School https://orcid.org/0000-0001-6964-9842

Ozge Erdogan
Harvard Medical School

Alec Walker
Boston Children's Hospital

Simone Carneiro-Nascimento
Beth Israel Deaconess Medical Center

Kathleen He
Harvard Medical School

Glendon Wu
Harvard Medical School

Beth Stevens
Boston Children's Hospital https://orcid.org/0000-0003-4226-1201

Kelly Doran
University of Colorado Anschutz Medical Campus

Dan Levy
Beth Israel Deaconess Medical Center

Biological Sciences - Article

Keywords:

Posted Date: March 25th, 2022

DOI: https://doi.org/10.21203/rs.3.rs-1479118/v1

Bacteria hijack a neuro-immune axis in the meninges to facilitate brain invasion

Felipe A. Pinho-Ribeiro[1], Liwen Deng[1], Dylan V. Neel[1], Ozge Erdogan[2], Alec J. Walker[3,4], Simone Carneiro-Nascimento[5], Kathleen He[1], Glendon Wu[1], Beth Stevens[3,4,6], Kelly S. Doran[7], Dan Levy[5], Isaac Chiu[1*]

[1]Department of Immunology, Blavatnik Institute, Harvard Medical School, Boston, MA, USA

[2]Department of Restorative Dentistry and Biomaterial Sciences, Harvard School of Dental Medicine, Boston, MA, USA

[3]F.M. Kirby Neurobiology Center, Boston Children's Hospital, and Harvard Medical School, Boston, MA, USA

[4]Stanley Center for Psychiatric Research, Broad Institute of MIT and Harvard, Cambridge, MA, USA

[5]Departments of Anesthesia, Critical Care and Pain Medicine, Beth Israel Deaconess Medical Center, Boston, MA, USA

[6]Howard Hughes Medical Institute, Boston Children's Hospital, Boston, MA, USA

[7]Department of Immunology and Microbiology, University of Colorado Anschutz Medical Campus, Aurora, CO, USA

*Corresponding author:

Isaac Chiu. Harvard Medical School. 77 Avenue Louis Pasteur, Boston, MA, 02115, USA.

Email: Isaac_chiu@hms.harvard.edu.

Abstract

The meninges are densely innervated by nociceptive sensory neurons that mediate pain and headache[1,2]. Bacterial meningitis is a life-threatening infection of the meninges and central nervous system (CNS) that affects over one million people a year[3-5]. However, whether pain and neuro-immune interactions impact CNS bacterial invasion is unclear. Here we find that nociceptor signaling to immune cells via the neuropeptide calcitonin gene-related peptide (CGRP) exacerbates bacterial meningitis. Nociceptor ablation reduced meningeal and brain invasion by two bacterial pathogens: *Streptococcus pneumoniae* and *Streptococcus agalactiae*. Bacteria directly activated nociceptors to release CGRP, which acts through its receptor RAMP1 on meningeal macrophages to inhibit chemokine expression and immune defenses. Macrophage-specific RAMP1 deficiency or blockade of RAMP1 signaling enhanced immune responses and bacterial clearance in the meninges and brain. Therefore, targeting a neuro-immune axis in the meninges can enhance host defenses and may be a potential treatment for bacterial meningitis.

Introduction

The meninges consist of three protective membranes (dura, arachnoid, pia) that surround the central nervous system (CNS), serving as a barrier that protects the brain and spinal cord from injury and infection[1]. However, some bacterial pathogens can invade the meningeal layers and subsequently enter the brain to cause pathology. Two of the leading causes of acute bacterial meningitis in humans are *Streptococcus pneumoniae* and *Streptococcus agalactiae* (also known as Group B *Streptococcus*, GBS). *S. pneumoniae* is a leading cause of meningitis in children, immunocompromised adults, and the elderly[4], while *S. agalactiae* is a leading cause of neonatal meningitis [4,6]. Bacterial meningitis is life-threatening, with mortality rates up to 30%, and even with successful treatment up to 50% of survivors have post-infectious neurological sequelae[4,7]. There is a need to better understand host responses to these bacteria, including defining the key players that mediate meningeal inflammation and bacterial invasion of the CNS. Nociceptors are peripheral sensory neurons that detect noxious/harmful stimuli and mediate the unpleasant sensation of pain. Our group and others have demonstrated that nociceptors communicate with immune cells in other barrier sites such as the skin [8-13]. Bacterial meningitis is accompanied by acute headache[3,5,7,14]. The meninges are densely innervated by trigeminal nociceptors that mediate headache and migraine[15,16]. Recent work has also defined a repertoire of innate and adaptive immune cells within the dural meninges that play roles in wound healing, sampling antigens from the CNS, and host defense [17-24]. However, the role of pain and neuro-immune signaling within the meningeal barrier has not been clearly defined in host defense.

Nociceptive neurons control *S. pneumoniae* and *S. agalactiae* invasion of the meninges and brain

We hypothesized that nociceptors may actively participate in meningeal host defenses. Nav1.8 is a voltage-gated sodium channel that is broadly expressed by nociceptors that mediate mechanical, cold,

and inflammatory pain[25]. Calcitonin gene-related peptide (CGRP) is a neuropeptide stored in dense core vesicles in nociceptor nerve terminals that mediates headache and migraine [16,26]. We performed confocal imaging of the meninges and found dense innervation by nerve fibers that were positive for both Nav1.8 and CGRP (**Fig. 1a**). To determine the role of these neurons in bacterial host defense, we utilized murine models of *S. pneumoniae* and *S. agalactiae* bacterial meningitis. In humans, the main route of CNS invasion by bacterial pathogens is via hematogenous spread to the brain [27]. We injected mice intravenously with *S. pneumoniae* or *S. agalactiae,* and isolated meningeal and brain tissues to analyze the time course of CNS invasion (**Fig. 1b**). In mice infected with *S. pneumoniae,* bacteria first reached the dura mater (outer layer of meninges) by 6h, and subsequently the inner meningeal layers (pia, arachnoid), choroid plexus (ChP), and brain by 24h (**Fig. 1c** and **Extended Data Fig. 1a**). In mice infected with *S. agalactiae*, we observed bacterial invasion of the dura mater and pia/arachnoid by 12h, followed by the brain by 24h (**Fig. 1d**). These data indicate that the dura mater is densely innervated by nociceptors and is an early step towards brain invasion for both bacterial pathogens.

We next targeted nociceptors using genetic and pharmacological tools to determine their roles in the pathogenesis of bacterial meningitis. *Nav1.8-cre* mice were bred with *Cre*-dependent Diphtheria Toxin A (DTA) mice to generate Nav1.8-DTA (Nav1.8-Cre^{+}/DTA^{+}) nociceptor ablated mice and Cre^{-} control littermates (**Fig. 1e**). Nav1.8-DTA mice lacking nociceptors and littermate controls were infected with *S. pneumoniae* and *S. agalactiae*, followed by the analysis of bacterial load recovery from the meninges and brain. Nav1.8-DTA mice developed less severe *S. pneumoniae* infection compared with control mice, with significantly lower bacterial loads recovered from the meninges (dura, pia/arachnoid/ChP) and brain at 24 h and 48 h post-infection (**Fig. 1f** and **Extended Data Fig. 1b**). By contrast, we did not observe differences in bacterial load in blood or peripheral tissues including spleen, liver, and skin (**Fig. 1f** and **Extended Data Fig. 1b, c)**. Nav1.8-DTA mice also showed significantly decreased meningeal and brain infection by *S. agalactiae* compared to control littermates at 24 h post-infection (**Fig. 1g**). Brain samples

collected after *S. pneumoniae* infection showed that Nav1.8-DTA mice had decreased pathology compared to control littermates, with reduced cleaved caspase-3 staining and histopathological damage (**Extended Data Fig. 1d**, **e**). As a second strategy to target nociceptors, we performed chemical ablation of nociceptors by treating mice with resiniferatoxin (RTX), a high-affinity agonist for the TRPV1 ion channel, which induces denervation and ablation of nociceptors[10]. Mice were treated with either RTX or vehicle, rested for 4 weeks, and subsequently infected with *S. pneumoniae*. RTX-treated mice showed significantly less *S. pneumoniae* bacterial invasion of meninges and brain compared to vehicle-treated control mice, phenocopying results using Nav1.8-DTA mice (**Extended Data Fig. 1f**). Given that the dura mater is an early site of bacterial infection and displays dense nociceptor innervation (**Fig. 1a-d**), we hypothesized that nociceptors regulate dural host defenses prior to bacterial entry into the brain. When bacteria were injected via the intracisternal route into the subarachnoid space, thereby bypassing the dura mater, Nav1.8-DTA and control mice no longer showed differences in bacterial load recovery (**Extended Data Fig. 1g**). Thus, dural nociceptors regulate CNS bacterial invasion following systemic infection, and ablating these nociceptors enhances bacterial clearance in the meninges and brain.

We hypothesized that nociceptors may regulate the meningeal immune response during bacterial invasion. *S. pneumoniae* infection caused increases in total meningeal leukocytes ($CD45^+$) in the dura, including neutrophils ($CD11b^+Ly6G^+$) and monocytes ($CD11b^+Ly6G^-Ly6C^{hi}$) over time (**Extended Data Fig. 2a**). Compared to control littermates, *Nav1.8-DTA* mice showed significantly increased meningeal leukocyte numbers following *S. pneumoniae* infection, with greater recruitment of both myeloid immune cells (macrophages, neutrophils, monocytes) and lymphocytes (B and T cells) (**Fig. 1h** and **Extended Data Fig. 2b**)**.** MRC1 (mannose receptor C-type 1) is expressed by meningeal macrophages that respond to traumatic brain injury and infection[19,20]. $CD11b^+MRC1^+$ meningeal macrophages were significantly increased in Nav1.8-DTA mice compared to control littermates in *S. pneumoniae* infected mice (**Fig. 1h**). Neutrophils are key host responders to bacterial infection, increasing in cerebrospinal fluid of meningitis

patients[27,28]. The numbers of $CD11b^{+}Ly6G^{+}$ neutrophils also increased significantly in Nav1.8-DTA mice compared to littermate controls following bacterial infection (**Fig. 1h**). Together, these results indicate that nociceptors may play a role in decreasing meningeal immune cell recruitment and bacterial clearance in response to infection.

Bacteria directly activate nociceptors to release the neuropeptide CGRP

Bacterial meningitis is characterized by severe headache and pain[3,5,7,14]. Yet the mechanisms leading to nociceptor activation during bacterial meningitis have not been explored. Grimace scores are a measure of pain in mouse models of headache [29]. We found that mice with bacterial meningitis exhibited increased grimace scores compared to uninfected mice for both *S. pneumoniae* and *S. agalactiae* (**Extended data Fig. 3a**). Nociceptor activation causes the release of neuropeptides including CGRP from peripheral terminals in the dural meninges, which is thought to mediate headache [9,16,26,29]. The intensity of headache caused by infection was comparable to that induced by systemic CGRP injection (**Extended Data Fig. 3b**), which has been used to model migraine headache in mice[29]. In addition to mediating pain, CGRP can also signal to immune cells and regulate their functions[9]. We next asked whether bacterial meningitis induces CGRP release in the meninges. Using meningeal explants (**Fig. 2a**), we observed increased levels of soluble CGRP released over the time course of *S. pneumoniae* infection (**Fig. 2b**). Nav1.8-DTA mice showed decreased CGRP release compared to control littermates after infection, indicating that nociceptors are a major source of CGRP released during infection (**Fig. 2c**). Infection with *S. agalactiae* also induced release of CGRP in the meninges (**Fig. 2d**). These results demonstrate that bacterial meningitis is associated with local CGRP release that may contribute to bacterial CNS invasion. When mice were infected with fluorescently labeled bacteria, CGRP+ nerve fibers were often juxtaposed with *S. pneumoniae* and *S.*

agalactiae in the dural meninges (**Fig. 2e**). This proximity hints at potential neuron-bacteria interactions during infection.

We next asked whether these bacterial pathogens can directly activate meningeal nociceptors to release CGRP. The meninges are innervated by nociceptors whose cell bodies reside in the trigeminal ganglia (TG). The release of CGRP from peripheral terminals of nociceptors occurs through a mechanism that is triggered by increases in intracellular calcium[9]. Using Fura-2 ratiometric imaging, we found that TG neurons directly responded to *S. pneumoniae* as measured by calcium influx, with increasing bacterial concentrations activating greater proportions of neurons ($4x10^5$-$4x10^7$ c.f.u./ml) (**Fig. 2f**). Capsaicin, the pungent ingredient in chili peppers that activates the nociceptive ion channel TRPV1[30], was used to identify the nociceptor population (capsaicin+) in the culture of TG sensory neurons. We confirmed that many bacterial-responsive neurons also responded to capsaicin. *S. pneumoniae* was also able to induce CGRP release from TG neurons (**Fig. 2g**). Similarly, we found that *S. agalactiae* ($2x10^7$-$2x10^9$ c.f.u./mL) also activated TG nociceptor (capsaicin +) neurons (**Fig. 2h**) and induced neuronal release of CGRP *in vitro* (**Fig. 2i**). These data confirm that both bacterial pathogens produce factors that can act on nociceptors to trigger calcium influx and CGRP release.

We had previously found that bacterial pore-forming toxins including alpha-hemolysin from *Staphylococcus aureus* and Streptolysin S from *Streptococcus pyogenes* can directly activate nociceptors and drive pain [10,31]. *S. pneumoniae* utilizes pneumolysin (PLY), a cholesterol-dependent cytolysin, as a major virulence factor for the invasion of host tissues including the lungs and the meninges[27,32,33]. We found that WT *S. pneumoniae* induced significantly more calcium influx compared to isogenic mutant bacteria lacking pneumolysin (Δ*ply*) (**Fig. 2j**). We asked whether PLY was able to directly activate nociceptors. Recombinant PLY induced robust calcium influx and CGRP release in TG neurons in a dose-dependent manner (**Fig. 2k** and **2l**). Taken together, these data show that meningitis-inducing bacterial

pathogens directly activate nociceptors and induce CGRP release. For *S. pneumoniae*, one molecular mechanism of nociceptor activation and CGRP release is via the pore-forming toxin PLY.

CGRP-RAMP1 signaling suppresses host defense during bacterial meningitis

Our group has recently described that CGRP contributes to the pathogenesis of necrotizing fasciitis, an invasive form of *S. pyogenes* infection that is also characterized by the presence of intense pain early in disease[10]. We hypothesized that signaling via CGRP could also plays a role in meningeal antibacterial host defenses. RAMP1 (receptor activity modifying protein 1) is a single-transmembrane-domain protein that, together with its coreceptor CALCRL (calcitonin-receptor-like receptor), forms the receptor complex that binds CGRP[34]. We found that *Ramp1*$^{-/-}$ mice showed significantly less bacterial invasion of the meninges and brain following *S. pneumoniae* inoculation compared to *Ramp1*$^{+/+}$ littermate controls (**Fig. 3a**). In line with our previous observations using nociceptor deficient mice (**Fig. 1h**), we also detected more immune cells, including macrophages and neutrophils in the meninges of infected *Ramp1*$^{-/-}$ mice compared with infected *Ramp1*$^{+/+}$ littermate controls (**Fig. 3b** and **Extended Data Fig. 4a**). On the other hand, systemic CGRP injection into wild-type mice potentiated *S. pneumoniae* invasion of the CNS and decreased the number of immune cells in the meninges (**Fig. 3c, d** and **Extended Data Fig. 4b)**. Treatment with CGRP also potentiated the invasion of the meninges and brain tissues by *S. agalactiae* (**Extended Data Fig. 4c**). In a pharmacological approach, mice were treated with BIBN4096S (olcegepant), an antagonist of mouse and human RAMP1 signaling [34,35]. RAMP1 antagonist treatment significantly reduced bacterial invasion into the meninges and brain compared to vehicle control (**Fig. 3e**). Given that RAMP1 antagonists are currently used to treat migraine in humans[26], these findings could have implications for also treating meningitis.

To determine whether meningeal immune cells are equipped to respond to CGRP, we performed single-cell RNA-sequencing analysis of meningeal CD45^{+} cells (**Fig. 4a**). The identity of each cluster was defined by comparing their transcriptional signature/cluster gene markers with previously published single-cell RNA-seq datasets of meningeal cells[17,23,24,36]. Matching these studies, we found a rich repertoire of myeloid and lymphoid cells populating the dural meninges at homeostasis (**Fig. 4a** and **Extended Data Fig. 5a**). We next analyzed meningeal immune populations for expression of neuropeptide receptors, which would allow them to directly receive signals from neuronal subtypes innervating the meninges. *Ramp1* and *Calcrl*, which are the genes encoding the two components that form CGRP receptor, ranked at the top of the list of neuropeptide receptors expressed in several meningeal immune cell clusters (**Fig. 4b**). Expression of other neuropeptide receptors were also identified, including adrenomedullin receptors *Ramp2* and *Ramp3*, VIP receptor *Vipr1,* substance P receptors *Tacr1* and *Mrgbrp2*, and PACAP receptor *Adcyap1r1*, though at much lower levels and less broadly compared to *Ramp1* (**Fig. 4b**). We did not detect the expression of other neuropeptide receptor genes, including receptors for other tachykinins (*Tacr2* and *Tacr3*) and neuromedin U (*Nmur1* and *Nmur2*). *Ramp1* was particularly highly expressed across myeloid immune cells including phagocytes (neutrophils, monocytes, macrophages) that also expressed Lysozyme M (positive for *Lyz2*), an antimicrobial enzyme that lyses bacterial cell membranes and kills both gram-positive and gram-negative bacteria (**Fig. 4c**).

We next asked which meningeal cell-types mediated RAMP1 signaling *in vivo* to impact bacterial meningitis. We bred tissue specific *Cre* lines with *Ramp1*^{floxed} mice to generate conditional knockout strains to interrogate the role of this receptor in distinct cell types. First, we bred *Lyz2-Cre* mice with Ramp1$^{fl/fl}$ to ablate the receptor in myeloid immune cells (**Fig. 4c, d**). Loss of *Ramp1* in myeloid cells (*Lyz2*$^{\Delta Ramp1}$) led to significantly reduced bacterial load in the meninges and brain following *S. pneumoniae* infection compared to control *Ramp1*$^{fl/fl}$ mice (**Fig. 4d**). We also performed single-cell RNA-sequencing analysis of CD45- non-immune cells of the meninges, finding that smooth muscle cells (positive for *Acta2*)

represented the main non-immune cell population expressing *Ramp1* and *Calcrl* (**Fig 4e** and **Extended Data Fig. 5b**). We next bred *Acta2*-Cre with *Ramp1*$^{fl/fl}$ mice to determine the role of Ramp1 in smooth muscle cells during *S. pneumoniae* infection. By contrast with *Lyz2-Cre* based myeloid immune cell Ramp1 ablation, *Acta2*$^{\Delta ramp1}$ mice did not show differences in bacterial recovery from the meninges or brain compared to control *Cre*- mice (**Fig 4f**). These data indicate that RAMP1 signaling in *Lyz2*+ myeloid immune cells but not *Acta2*+ smooth muscle cells suppress effective host defenses during bacterial meningitis.

Meningeal macrophages respond to infection and mediate host defense

Macrophages and other professional phagocytes like neutrophils and monocytes are well known to be critical for effective ingestion, killing and resolution of acute bacterial infections. Yet it remains poorly understood how these and other immune cells respond to bacterial infection and insults at the barriers of the CNS. To better understand the role of these cells in the host response during bacterial meningitis, we performed single-cell RNA-sequencing of CD45^{+} immune cells collected from dural meninges at 24h post *S. pneumoniae* infection and compared the datasets with immune cells collected from uninfected animals (**Fig. 5a** and **Extended Data Fig. 6a**). Transcriptional changes in response to infection were particularly abundant in the myeloid immune cell clusters composed of macrophages, monocytes, and neutrophils (**Extended data Fig. 6b**). Pathway enrichment analysis of differentially expressed genes in myeloid populations highlighted the roles of these cells in host responses to infection (**Fig. 5b** and **Extended data Fig. 6c-e**).

Macrophages are the most abundant immune cell type in the meninges and therefore may be the first to encounter and respond to bacteria. We were able to detect *S. pneumoniae* associated with meningeal Mrc1+ macrophages 24h post-injection (**Fig. 5c** and **Extended Data Fig. 7a**). In macrophages, we observed enrichment of biological processes related to the recruitment of immune cells due to the

increased expression of several mediators that promote chemotaxis of myeloid and lymphoid immune cells including *Ccl12*, *Ccl2*, *Ccl3, and Tnf* (**Extended Data Fig. 6c** and **Fig. 5b**). Therefore, macrophages may orchestrate meningeal protection by mediating the recruitment of immune cells that exert antimicrobial functions such as neutrophils and monocytes (**Extended Data Fig. 6d**, **e**).

We next depleted meningeal macrophages by performing intracisternal injection of clodronate-laden liposomes (CLL) or control liposomes. Confirming their importance in CNS immunity, depletion of meningeal macrophages using this approach (**Fig. 5d**) potentiated bacterial invasion of the meninges and brain (**Fig. 5e**) and resulted in a global reduction in the number of immune cells including neutrophils and monocytes recruited specifically to the meninges during *S. pneumoniae* infection (**Extended Data Fig. 7b**, **c**). We also found that dural CX3CR1+ macrophages were often in close association with CGRP+ nociceptors (**Fig 5f**). Therefore, we next investigated how CGRP-RAMP1 signaling impacts the function of meningeal macrophages during infection.

CGRP-RAMP1 signaling suppresses macrophage-mediated CNS immunity against bacterial infection

Because *Lyz2* is expressed in all myeloid cells including neutrophils, macrophages, and monocytes, we sought to identify a unique marker to target *Ramp1* expression specifically in meningeal macrophages to determine their role in infection. A recent study found that meningeal macrophages and other CNS border-associated macrophages expressed *Pf4* (the gene encoding CXCL4) and can be labeled using *Pf4-Cre* knock-in mice; *Pf4* was also found to be absent in microglial cells[37]. Our single-cell RNA-seq analysis of meningeal immune cells confirmed *Pf4* expression by a large proportion of CD11b+MRC1+ dural macrophages, but absent in neutrophils and monocytes (**Fig. 6a** and **Extended Data Fig. 6a**). When *Pf4-Cre* mice were bred with *Cre*-dependent TdTomato reporter mice, this resulted in labeling of macrophages associated with CGRP+ nerves and CD31+ blood vessels in the dural meninges (**Fig. 6b**). To target Ramp1

in macrophages, we next bred *Pf4*-cre with *Ramp1*$^{fl/fl}$ to generate mice lacking *Ramp1* specifically in these *Pf4*+ cells (*Pf4*$^{\Delta ramp1}$). Similar to the results observed in total myeloid-specific *Ramp1* knockout mice (*Lyz2*$^{\Delta ramp1}$) (**Fig 4d**), *Pf4*$^{\Delta ramp1}$ mice were less susceptible to meningeal and CNS infections by *S. pneumoniae* compared to control mice (**Fig. 6c**). Taken together, these data indicate that RAMP1 signaling in macrophages critically regulates meningeal host defenses.

To gain mechanistic insights into how CGRP directly impacts macrophage responses to *S. pneumoniae*, we utilized *in vitro* cultures of bone marrow-derived macrophages (BMDM). Macrophages were co-incubated with serum-opsonized *S. pneumoniae* (MOI 1) for 4h in the presence of CGRP (100 nM) or vehicle. We did not observe defects in the antimicrobial activity of macrophages exposed to CGRP (**Extended data Fig. 8a**). We next asked whether CGRP could induce major transcriptional changes in macrophages in response to bacterial infection by performing RNAseq analysis of cells treated with vehicle, bacteria alone, or both CGRP and bacteria (**Fig. 6d**). Compared to vehicle-treated cells, macrophages exposed to *S. pneumoniae* showed robust upregulation of cytokines and chemokines (**Fig. 6d**). In contrast, treatment with CGRP polarized bacteria-stimulated macrophage transcriptional phenotypes to a suppressed expression of cytokines including TNFα, CCL3, and CCL4 (**Fig. 6d**). We confirmed that protein levels of these cytokines were also significantly reduced by CGRP treatment during *S. pneumoniae* infection of macrophages (**Extended data Fig. 8b**). RAMP1/CALCRL forms a G protein-coupled receptor that signals via a Gαs subunit, which leads to increased intracellular levels of the second messenger cyclic AMP (cAMP) and activation of the cAMP-dependent protein kinase PKA[34]. To investigate the role of this pathway on the polarization of macrophages induced by CGRP, macrophages were treated with the cAMP analog Rp-8-CPT-cAMP, a site-selective inhibitor of PKA (PKAi), 3h prior to the application of CGRP and *S. pneumoniae*. In line with the RNAseq data, we confirmed by RT-qPCR that CGRP downregulates the expression of multiple chemotactic mediators (**Fig. 6e** and **Extended Data Fig. 8c**). This cytokine suppression activity of CGRP was blocked when cells were pretreated with PKAi (**Fig. 6e** and

Extended Data Fig. 8c). To determine whether CGRP has a similar impact on meningeal macrophages i*n vivo*, we performed single-cell RNA sequencing analysis of meningeal $CD45^+$ cells isolated from mice treated with CGRP or vehicle during infection with *S. pneumoniae* (**Fig. 6f**). We found that CGRP treatment had a profound impact on meningeal immune cell populations *in vivo*, with the greatest number of differentially expressed genes in the MRC1+PF4+ macrophage population (**Fig. 6f**). Pathway enrichment analysis showed that CGRP treatment in the context of bacterial meningitis had a major impact on the expression of genes involved in chemotaxis (**Fig. 6g**). In line with our hypothesis, we identified multiple chemokines that were downregulated by CGRP *in vivo* including *Ccl2* and *Cxcl10* (**Fig. 6g**) which overlapped with CGRP-downregulated genes we found *in vitro* (**Fig. 6h**). We also observed both *in vivo* and *in vitro* the upregulation of *Crem* (gene encoding Inducible cAMP Early Repressor, or ICER) and *Jdp2* (gene encoding Jun Dimerization Protein 2) (**Fig. 6d, g, h** and **Extended Data Fig. 8c**), two key transcription factors that have previously found to downregulate NFκB and cytokine expression in macrophages[38,39]. Collectively these data indicate that CGRP-RAMP1 signaling induces a transcriptional program in macrophages that blunts cytokine expression, *in vitro* and *in vivo*.

We next determined the impact of RAMP1 signaling on meningeal macrophages during infection using $Pf4^{\Delta ramp1}$ mice. Compared to control mice, macrophages isolated from the meninges of $Pf4^{\Delta ramp1}$ mice expressed higher transcript levels for chemotactic mediators (*Tnf*, *Ccl2*, *Ccl3*, and *Cxcl10*) (**Fig. 6i**). In contrast, the expression of anti-inflammatory genes *Crem* and *Jdp2*, as well as the *Ramp1* gene, were downregulated in $Pf4^{\Delta ramp1}$ mice (**Extended Data Fig. 8d**). Confirming the impact of CGRP and RAMP1 signaling on the macrophage-mediated recruitment of immune cells, the meninges of $Pf4^{\Delta ramp1}$ mice exhibited higher numbers of neutrophils and monocytes compared to control littermates (**Fig. 6j** and **Extended Data Fig. 8e**). These results uncover the existence of a neuro-immune axis in the meninges that modulates immune responses and reveal how bacterial pathogens exploit this signaling to suppress antimicrobial immunity (**Extended Data Fig. 9**).

Discussion

The neural control of immunity is an emerging area of research that holds great potential to transform our understanding of human diseases and to reveal novel therapeutic targets[9,40]. In the present study, we investigated the immunomodulatory activity of meningeal nociceptors, sensory neurons that mediate headache and migraine, and their impact on immune responses against infection in the brain. Severe headache is a frequent early symptom of bacterial meningitis, but the mechanisms and consequences of nociceptor activation were unknown[3-5,7,14]. Here we report that *S. pneumoniae* and *S. agalactiae*, two pathogens that make up the majority of cases of bacterial meningitis in humans, activate nociceptors to promote meninges and brain invasion, thereby linking sensory neurons to the pathogenesis of bacterial meningitis. Our findings also uncover a neuro-immune axis in the meninges where the sensory nervous system signals to macrophages to blunt host defense via the CGRP-RAMP1 pathway.

Barrier tissues such as the skin and the gut are innervated by nociceptors that mediate pain in response to the presence of noxious stimuli such as high temperature, protons, ATP, and tissue injury [9]. Pain evokes protective behavioral changes (e.g. withdrawal response) that halt exposure to a harmful situation and prevent or minimize tissue damage. The CNS has its own barrier tissue, the meninges. In contrast to the CNS parenchyma, the layers of the meninges, especially the dura mater, is innervated by nociceptors and contains a rich repertoire of immune cells and lymphatic vessels [1,16]. The findings described here suggest a role for this intracranial nociceptive innervation in controlling the activity of meningeal immune cells and leukocyte trafficking. We show that depletion of Nav1.8+ and TRPV1+ nociceptors protect mice from CNS invasion by pathogens that cause human bacterial meningitis. This effect of nociceptors was specific to the initial steps of CNS infection when bacteria cross from blood to the meninges and not after bacteria has reached the brain, fitting with the existence of a neuro-immune

axis in the dura mater. A positive correlation between pain intensity and the severity of bacterial meningitis has been previously described in clinical and pre-clinical studies [3,7,14]. Our findings link nociceptor activation to infection pathogenesis due to neuronal suppression of innate immunity through meningeal CGRP signaling. We show that depletion of nociceptors results in reduced bacterial numbers in the meninges and the brain and decreased cortical pathology. These protective effects are associated with a global increase in the numbers of meningeal immune cells including neutrophils and macrophages. Nociceptors positively or negatively regulate leukocyte trafficking in other barrier tissues including the skin and the lungs depending on the inflammatory context [10,12,13,31]. Our study provides further evidence that supports the immunomodulatory activity of nociceptors.

Although the physiological role of this meningeal neuro-immune axis beyond infection remains unclear, it may represent a strategy to limit meningeal inflammation that can cause CNS pathology. Nociceptors are sensitive to inflammatory mediators produced by immune cells such as prostaglandin E2 and TNFα, which act on receptors expressed by these neurons to trigger pain hypersensitivity [9,41]. A nociceptor-driven downregulation of immune responses may provide negative feedback that limits the deleterious effects of excessive inflammation to promote tissue healing. Consistent with this hypothesis, nociceptors limit the intensity and the duration of inflammation in the lungs and joints, protecting these tissues from chronic inflammation and *function laesa*[42-44]. Nociceptors also support wound healing following injury in the skin and oral mucosa[45-48]. On the other hand, tumor cells and bacterial pathogens can benefit from the immunomodulatory activity of sensory innervation [10,11,13,31,49-52]. Herein, we describe two human bacterial pathogens that seem to exploit the immunomodulatory activity of nociceptors in the meninges to evade immunity and promote CNS invasion during bacterial meningitis.

We find that *S. pneumoniae* and *S. agalactiae* can directly activate nociceptors and induce CGRP release. One mechanism by which this neuronal activation occurs is through the pore-forming toxin Pneumolysin (PLY) produced by *S. pneumoniae*. PLY is a cholesterol-dependent cytolysin that plays a

critical role in the pathogenesis of bacterial meningitis[33,53,54]. Previous studies show that PLY can act on both human and murine brain neurons to induce neurotoxicity[55-58]. We find that PLY can also directly activate nociceptors to induce calcium influx and neuropeptide release that impacts downstream immunity. The activation of trigeminal nociceptors by either live bacteria or PLY was especially evident in the population of capsaicin-responsive cells, which labels TRPV1+ nociceptors. It remains to be determined how PLY binds to and targets nociceptors. We previously found that during subcutaneous infections, the gram-positive bacterial pathogen *S. pyogenes* activates TRPV1+ neurons by secreting the toxin Streptolysin S[10], and a second pathogen *S. aureus* activates nociceptors through the pore-forming toxin alpha-hemolysin to produce pain [10,31,59]. A common feature of these toxins is their ability to form large pores in the cell membrane, leading to ionic influx. For nociceptors, calcium and sodium influx induces firing of action potentials and SNARE-dependent release of neuropeptides including CGRP. In the meninges, peripheral nerve fibers of peptidergic nociceptors store large dense-core vesicles containing CGRP, which are quickly released in response to elevated intracellular calcium. Notably, human patients presenting with bacterial meningitis show significantly increased levels of CGRP in the cerebrospinal fluid and blood [14,60]. We confirmed the release of CGRP from the meninges in our models of bacterial meningitis.

We found that nociceptors signal via CGRP to meningeal PF4+MRC1+ macrophages, which critically regulate the outcome of bacterial meningitis. The CGRP receptor RAMP1 and its co-receptor CALCRL are widely expressed in the immune system. RAMP1/CALCRL forms a GPCR that signals through the Gαs subunit, which leads to adenylyl cyclase-mediated production of the second messenger cAMP and activation of PKA[34]. In the context of bacterial infection, upregulation of cAMP through virulence factors such as pertussis toxin and cholera toxin suppress leukocyte recruitment [61]. We show that CGRP signaling through this canonical cAMP-PKA pathway polarizes macrophages and their response to *S. pneumoniae*, inhibiting the production of chemotactic factors (e.g. *Ccl2*, *Ccl3*, *Tnf*) and upregulating the

expression of immunosuppressive transcriptional factors (e.g. *Crem*, *Jdp2*, *Nfkbi*). Increased cAMP levels have also been shown to counteract the chemokine signaling through Gαi GPCR, which results in inhibition of chemotaxis and contributes to increased pathogenesis during bacterial infections[9,61].

Neuron-macrophage crosstalk play key roles in host defense in other barrier sites including the gut and skin. In the gut, sympathetic neurons maintain muscularis macrophages in an anti-inflammatory transcriptional state and tissue-protective phenotype through the release of noradrenaline and activation of Beta-2 adrenergic receptors expressed in the macrophages [62,63]. Beta-2 adrenergic receptor, like RAMP1, signals through Gαs, and cAMP mediates gut macrophage polarization to a tissue-protective phenotype [61]. In the skin, the neuropeptide TAFA4 produced by GINIP+ sensory neurons stimulate the production of IL-10 by dermal macrophages to promote tissue healing.[64] Thus, it is possible that CGRP+ meningeal nociceptors signal to RAMP1+ macrophages in order to promote wound healing and resolution of inflammation in the CNS. In the context of bacterial meningitis, we find that this neuron-macrophage crosstalk impairs bacterial clearance in the CNS, suggesting that some pathogens may trigger early activation of this neuro-immune axis to evade meningeal immunity.

The crosstalk between meningeal nociceptors and macrophages may explain the association between headache and disease severity in patients with bacterial meningitis[3,7]. Currently, small molecule RAMP1 antagonists and antibodies against CGRP are used widely for the prevention and treatment of migraine in humans. Therefore, our observation that BIBN4096, an antagonist of RAMP1, ameliorates bacterial meningitis in mice caused by both *S. pneumoniae* and *S. agalactiae* in the CNS holds potential for therapeutic translation.

Recent studies have identified resident niches of neutrophils, B cells, and other immune cells in the skull bone marrow that traffic to the meninges through specialized channels during homeostasis and following inflammation[65,66,67]. Functional roles of the skull bone marrow in bacterial meningitis remains

undefined. It would be interesting to determine whether nociceptors impact these bone marrow immune populations and their trafficking to the meninges in future studies.

The meninges are classically defined as the barrier tissue that protects the CNS, which is based on the anatomorphological characteristics of this structure that surrounds the brain and the spinal cord. Despite this assumption, our knowledge about the cellular and molecular components of the meninges and how they interact to mediate tissue protection or host defense is limited. We uncover the existence of a neuro-immune axis in the meninges where nociceptors modulate the activity of meningeal immune cells. Bacterial pathogens hijack this axis to facilitate CNS invasion, highlighting the complexities of host-pathogen interactions and neuroimmune crosstalk. In light of recent breakthroughs demonstrating the impact of meningeal immune cells in health and disease of the CNS[1,18,20,22,24,68,69], our current study suggests that nociceptors could potentially affect the function of the CNS and play roles beyond bacterial meningitis. Therefore, future research on this topic could lead to the development of new treatments for infectious and other CNS diseases by targeting the peripheral nervous system.

References

1 Alves de Lima, K., Rustenhoven, J. & Kipnis, J. Meningeal Immunity and Its Function in Maintenance of the Central Nervous System in Health and Disease. *Annu Rev Immunol* **38**, 597-620, doi:10.1146/annurev-immunol-102319-103410 (2020).

2 Levy, D., Labastida-Ramirez, A. & MaassenVanDenBrink, A. Current understanding of meningeal and cerebral vascular function underlying migraine headache. *Cephalalgia* **39**, 1606-1622, doi:10.1177/0333102418771350 (2019).

3 Ostergaard, C., Konradsen, H. B. & Samuelsson, S. Clinical presentation and prognostic factors of *Streptococcus pneumoniae* meningitis according to the focus of infection. *BMC Infect Dis* **5**, 93, doi:10.1186/1471-2334-5-93 (2005).

4 van de Beek, D., Brouwer, M. C., Koedel, U. & Wall, E. C. Community-acquired bacterial meningitis. *Lancet* **398**, 1171-1183, doi:10.1016/S0140-6736(21)00883-7 (2021).

5 Lampl, C., Yazdi, K., Buzath, A. & Klingler, D. Migraine-like headache in bacterial meningitis. *Cephalalgia* **20**, 738-739, doi:10.1111/j.1468-2982.2000.00110.x (2000).

6 Doran, K. S. & Nizet, V. Molecular pathogenesis of neonatal group B streptococcal infection: no longer in its infancy. *Mol Microbiol* **54**, 23-31, doi:10.1111/j.1365-2958.2004.04266.x (2004).

7 van de Beek, D. *et al.* Clinical features and prognostic factors in adults with bacterial meningitis. *N Engl J Med* **351**, 1849-1859, doi:10.1056/NEJMoa040845 (2004).

8 Zhang, S. *et al.* Nonpeptidergic neurons suppress mast cells via glutamate to maintain skin homeostasis. *Cell* **184**, 2151-2166 e2116, doi:10.1016/j.cell.2021.03.002 (2021).

9 Pinho-Ribeiro, F. A., Verri, W. A., Jr. & Chiu, I. M. Nociceptor Sensory Neuron-Immune Interactions in Pain and Inflammation. *Trends Immunol* **38**, 5-19, doi:10.1016/j.it.2016.10.001 (2017).

10 Pinho-Ribeiro, F. A. *Et al.* Blocking Neuronal Signaling to Immune Cells Treats Streptococcal Invasive Infection. *Cell* **173**, 1083-1097 e1022, doi:10.1016/j.cell.2018.04.006 (2018).

11 Lin, T. *et al.* Pseudomonas aeruginosa-induced nociceptor activation increases susceptibility to infection. *PloS Pathog* **17**, e1009557, doi:10.1371/journal.ppat.1009557 (2021).

12 La Russa, F. *et al.* Disruption of the Sensory System Affects Sterile Cutaneous Inflammation In Vivo. *J Invest Dermatol* **139**, 1936-1945 e1933, doi:10.1016/j.jid.2019.01.037 (2019).

13 Baral, P. *Et al.* Nociceptor sensory neurons suppress neutrophil and gammadelta T cell responses in bacterial lung infections and lethal pneumonia. *Nat Med* **24**, 417-426, doi:10.1038/nm.4501 (2018).

14 Hoffmann, O. *et al.* Triptans reduce the inflammatory response in bacterial meningitis. *J Cereb Blood Flow Metab* **22**, 988-996, doi:10.1097/00004647-200208000-00010 (2002).

15 RAY, B. S. & WOLFF, H. G. EXPERIMENTAL STUDIES ON HEADACHE: PAIN-SENSITIVE STRUCTURES OF THE HEAD AND THEIR SIGNIFICANCE IN HEADACHE. *Archives of Surgery* **41**, 813-856, doi:10.1001/archsurg.1940.01210040002001 (1940).

16 Strassman, A. M. & Levy, D. Response properties of dural nociceptors in relation to headache. *J Neurophysiol* **95**, 1298-1306, doi:10.1152/jn.01293.2005 (2006).

17 Van Hove, H. *et al.* A single-cell atlas of mouse brain macrophages reveals unique transcriptional identities shaped by ontogeny and tissue environment. *Nat Neurosci* **22**, 1021-1035, doi:10.1038/s41593-019-0393-4 (2019).

18 Rustenhoven, J. *et al.* Functional characterization of the dural sinuses as a neuroimmune interface. *Cell* **184**, 1000-1016 e1027, doi:10.1016/j.cell.2020.12.040 (2021).

19 Russo, M. V. & McGavern, D. B. Inflammatory neuroprotection following traumatic brain injury. *Science* **353**, 783-785, doi:10.1126/science.aaf6260 (2016).

20 Rua, R. *et al.* Infection drives meningeal engraftment by inflammatory monocytes that impairs CNS immunity. *Nat Immunol* **20**, 407-419, doi:10.1038/s41590-019-0344-y (2019).

21 Mastorakos, P., Russo, M. V., Zhou, T., Johnson, K. & McGavern, D. B. Antimicrobial immunity impedes CNS vascular repair following brain injury. *Nat Immunol* **22**, 1280-1293, doi:10.1038/s41590-021-01012-1 (2021).

22 Fitzpatrick, Z. *et al.* Gut-educated IgA plasma cells defend the meningeal venous sinuses. *Nature* **587**, 472-476, doi:10.1038/s41586-020-2886-4 (2020).

23 Brioschi, S. *et al.* Heterogeneity of meningeal B cells reveals a lymphopoietic niche at the CNS borders. *Science* **373**, doi:10.1126/science.abf9277 (2021).

24 Alves de Lima, K. *Et al.* Meningeal gammadelta T cells regulate anxiety-like behavior via IL-17a signaling in neurons. *Nat Immunol* **21**, 1421-1429, doi:10.1038/s41590-020-0776-4 (2020).

25 Abrahamsen, B. *et al.* The cell and molecular basis of mechanical, cold, and inflammatory pain. *Science* **321**, 702-705, doi:10.1126/science.1156916 (2008).

26 Russo, A. F. Calcitonin gene-related peptide (CGRP): a new target for migraine. *Annu Rev Pharmacol Toxicol* **55**, 533-552, doi:10.1146/annurev-pharmtox-010814-124701 (2015).

27 Dando, S. J. *et al.* Pathogens penetrating the central nervous system: infection pathways and the cellular and molecular mechanisms of invasion. *Clin Microbiol Rev* **27**, 691-726, doi:10.1128/CMR.00118-13 (2014).

28 Mildner, A. *et al.* Ly-6G+CCR2- myeloid cells rather than Ly-6ChighCCR2+ monocytes are required for the control of bacterial infection in the central nervous system. *J Immunol* **181**, 2713-2722, doi:10.4049/jimmunol.181.4.2713 (2008).

29 Rea, B. J. *et al.* Peripherally administered calcitonin gene-related peptide induces spontaneous pain in mice: implications for migraine. *Pain* **159**, 2306-2317, doi:10.1097/j.pain.0000000000001337 (2018).

30 Caterina, M. J. *et al.* The capsaicin receptor: a heat-activated ion channel in the pain pathway. *Nature* **389**, 816-824, doi:10.1038/39807 (1997).

31 Chiu, I. M. *et al.* Bacteria activate sensory neurons that modulate pain and inflammation. *Nature* **501**, 52-57, doi:10.1038/nature12479 (2013).

32 Wippel, C. *et al.* Bacterial cytolysin during meningitis disrupts the regulation of glutamate in the brain, leading to synaptic damage. *PloS Pathog* **9**, e1003380, doi:10.1371/journal.ppat.1003380 (2013).

33 Reiss, A. *et al.* Bacterial pore-forming cytolysins induce neuronal damage in a rat model of neonatal meningitis. *J Infect Dis* **203**, 393-400, doi:10.1093/infdis/jiq047 (2011).

34 Arkless, K., Argunhan, F. & Brain, S. D. CGRP Discovery and Timeline. *Handb Exp Pharmacol* **255**, 1-12, doi:10.1007/164_2018_129 (2019).

35 Olesen, J. *et al.* Calcitonin gene-related peptide receptor antagonist BIBN 4096 BS for the acute treatment of migraine. *N Engl J Med* **350**, 1104-1110, doi:10.1056/NEJMoa030505 (2004).

36 Jordao, M. J. C. *Et al.* Single-cell profiling identifies myeloid cell subsets with distinct fates during neuroinflammation. *Science* **363**, doi:10.1126/science.aat7554 (2019).

37 McKinsey, G. L. *et al.* A new genetic strategy for targeting microglia in development and disease. *Elife* **9**, doi:10.7554/eLife.54590 (2020).

38 Harzenetter, M. D. *et al.* Negative regulation of TLR responses by the neuropeptide CGRP is mediated by the transcriptional repressor ICER. *J Immunol* **179**, 607-615, doi:10.4049/jimmunol.179.1.607 (2007).

39 Maruyama, K. *et al.* Nociceptors Boost the Resolution of Fungal Osteoinflammation via the TRP Channel-CGRP-Jdp2 Axis. *Cell Rep* **19**, 2730-2742, doi:10.1016/j.celrep.2017.06.002 (2017).

40 Pavlov, V. A., Chavan, S. S. & Tracey, K. J. Molecular and Functional Neuroscience in Immunity. *Annu Rev Immunol* **36**, 783-812, doi:10.1146/annurev-immunol-042617-053158 (2018).

41 Zhang, X. C., Kainz, V., Burstein, R. & Levy, D. Tumor necrosis factor-α induces sensitization of meningeal nociceptors mediated via local COX and p38 MAP kinase actions. *Pain* **152**, 140-149, doi: 10.1016/j.pain.2010.10.002 (2011).

42 Borbely, E. *et al.* Capsaicin-sensitive sensory nerves exert complex regulatory functions in the serum-transfer mouse model of autoimmune arthritis. *Brain Behav Immun* **45**, 50-59, doi:10.1016/j.bbi.2014.12.012 (2015).

43 Strausbaugh, H. J. *et al.* Painful stimulation suppresses joint inflammation by inducing shedding of L-selectin from neutrophils. *Nat Med* **5**, 1057-1061, doi:10.1038/12497 (1999).

44 Sterner-Kock, A. *et al.* Neonatal capsaicin treatment increases the severity of ozone-induced lung injury. *Am J Respir Crit Care Med* **153**, 436-443, doi:10.1164/ajrccm.153.1.8542155 (1996).

45 Lambiase, A. *et al.* Capsaicin-induced corneal sensory denervation and healing impairment are reversed by NGF treatment. *Invest Ophthalmol Vis Sci* **53**, 8280-8287, doi:10.1167/iovs.12-10593 (2012).

46 Martinez-Martinez, E., Galvan-Hernandez, C. I., Toscano-Marquez, B. & Gutierrez-Ospina, G. Modulatory role of sensory innervation on hair follicle stem cell progeny during wound healing of the rat skin. *PloS One* **7**, e36421, doi:10.1371/journal.pone.0036421 (2012).

47 Smith, P. G. & Liu, M. Impaired cutaneous wound healing after sensory denervation in developing rats: effects on cell proliferation and apoptosis. *Cell Tissue Res* **307**, 281-291, doi:10.1007/s00441-001-0477-8 (2002).

48 Byers, M. R. & Taylor, P. E. Effect of sensory denervation on the response of rat molar pulp to exposure injury. *J Dent Res* **72**, 613-618, doi:10.1177/00220345930720031001 (1993).

49 Kappos, E. A. *et al.* Denervation leads to volume regression in breast cancer. *J Plast Reconstr Aesthet Surg* **71**, 833-839, doi:10.1016/j.bjps.2018.03.012 (2018).

50 Amit, M. *et al.* Loss of p53 drives neuron reprogramming in head and neck cancer. *Nature* **578**, 449-454, doi:10.1038/s41586-020-1996-3 (2020).

51 Peterson, S. C. *et al.* Basal cell carcinoma preferentially arises from stem cells within hair follicle and mechanosensory niches. *Cell Stem Cell* **16**, 400-412, doi:10.1016/j.stem.2015.02.006 (2015).

52 Saloman, J. L. *et al.* Ablation of sensory neurons in a genetic model of pancreatic ductal adenocarcinoma slows initiation and progression of cancer. *Proc Natl Acad Sci U S A* **113**, 3078-3083, doi:10.1073/pnas.1512603113 (2016).

53 Hirst, R. A., Kadioglu, A., O'Callaghan, C. & Andrew, P. W. The role of pneumolysin in pneumococcal pneumonia and meningitis. *Clin Exp Immunol* **138**, 195-201, doi:10.1111/j.1365-2249.2004.02611.x (2004).

54 Wellmer, A. *et al.* Decreased virulence of a pneumolysin-deficient strain of *Streptococcus pneumoniae* in murine meningitis. *Infect Immun* **70**, 6504-6508, doi:10.1128/IAI.70.11.6504-6508.2002 (2002).

55 Braun, J. S. *et al.* Pneumolysin causes neuronal cell death through mitochondrial damage. *Infect Immun* **75**, 4245-4254, doi:10.1128/IAI.00031-07 (2007).

56 Stringaris, A. K. *et al.* Neurotoxicity of pneumolysin, a major pneumococcal virulence factor, involves calcium influx and depends on activation of p38 mitogen-activated protein kinase. *Neurobiol Dis* **11**, 355-368, doi:10.1006/nbdi.2002.0561 (2002).

57 Braun, J. S. *et al.* Pneumococcal pneumolysin and H(2)O(2) mediate brain cell apoptosis during meningitis. *J Clin Invest* **109**, 19-27, doi:10.1172/JCI12035 (2002).

58 Tabusi, M. *et al.* Neuronal death in pneumococcal meningitis is triggered by pneumolysin and RrgA interactions with beta-actin. *PloS Pathog* **17**, e1009432, doi:10.1371/journal.ppat.1009432 (2021).

59 Higashi, D. L. *et al.* Activation of band 3 mediates group A Streptococcus streptolysin S-based beta-haemolysis. *Nat Microbiol* **1**, 15004, doi:10.1038/nmicrobiol.2015.4 (2016).

60 Berg, R. M. *et al.* Circulating levels of vasoactive peptides in patients with acute bacterial meningitis. *Intensive Care Med* **35**, 1604-1608, doi:10.1007/s00134-009-1515-3 (2009).

61 Serezani, C. H., Ballinger, M. N., Aronoff, D. M. & Peters-Golden, M. Cyclic AMP: master regulator of innate immune cell function. *Am J Respir Cell Mol Biol* **39**, 127-132, doi:10.1165/rcmb.2008-0091TR (2008).

62 Gabanyi, I. *et al.* Neuro-immune Interactions Drive Tissue Programming in Intestinal Macrophages. *Cell* **164**, 378-391, doi:10.1016/j.cell.2015.12.023 (2016).

63 Matheis, F. *et al.* Adrenergic Signaling in Muscularis Macrophages Limits Infection-Induced Neuronal Loss. *Cell* **180**, 64-78 e16, doi:10.1016/j.cell.2019.12.002 (2020).

64 Hoeffel, G. *et al.* Sensory neuron-derived TAFA4 promotes macrophage tissue repair functions. *Nature* **594**, 94-99, doi:10.1038/s41586-021-03563-7 (2021).

65 Herisson, F., *et al*. Direct vascular channels connect skull bone marrow and the brain surface enabling myeloid cell migration. *Nat Neurosci* **21**, 1209-1217. doi: 10.1038/s41593-018-0213-2 (2018).

66 Cugurra, A. *et al*. Skull and vertebral bone marrow are myeloid cell reservoirs for the meninges and CNS parenchyma. *Science* **373**, eabf7844. doi: 10.1126/science.abf7844 (2021).

67 Brioschi, S. *et al*. Heterogeneity of meningeal B cells reveals a lymphopoietic niche at the CNS borders. Science **373**, eabf9277. doi: 10.1126/science.abf9277 (2021).

68 Da Mesquita, S. *et al.* Meningeal lymphatics affect microglia responses and anti-Abeta immunotherapy. *Nature* **593**, 255-260, doi:10.1038/s41586-021-03489-0 (2021).

69 Song, E. *et al.* VEGF-C-driven lymphatic drainage enables immunosurveillance of brain tumours. *Nature* **577**, 689-694, doi:10.1038/s41586-019-1912-x (2020).

Figure 1

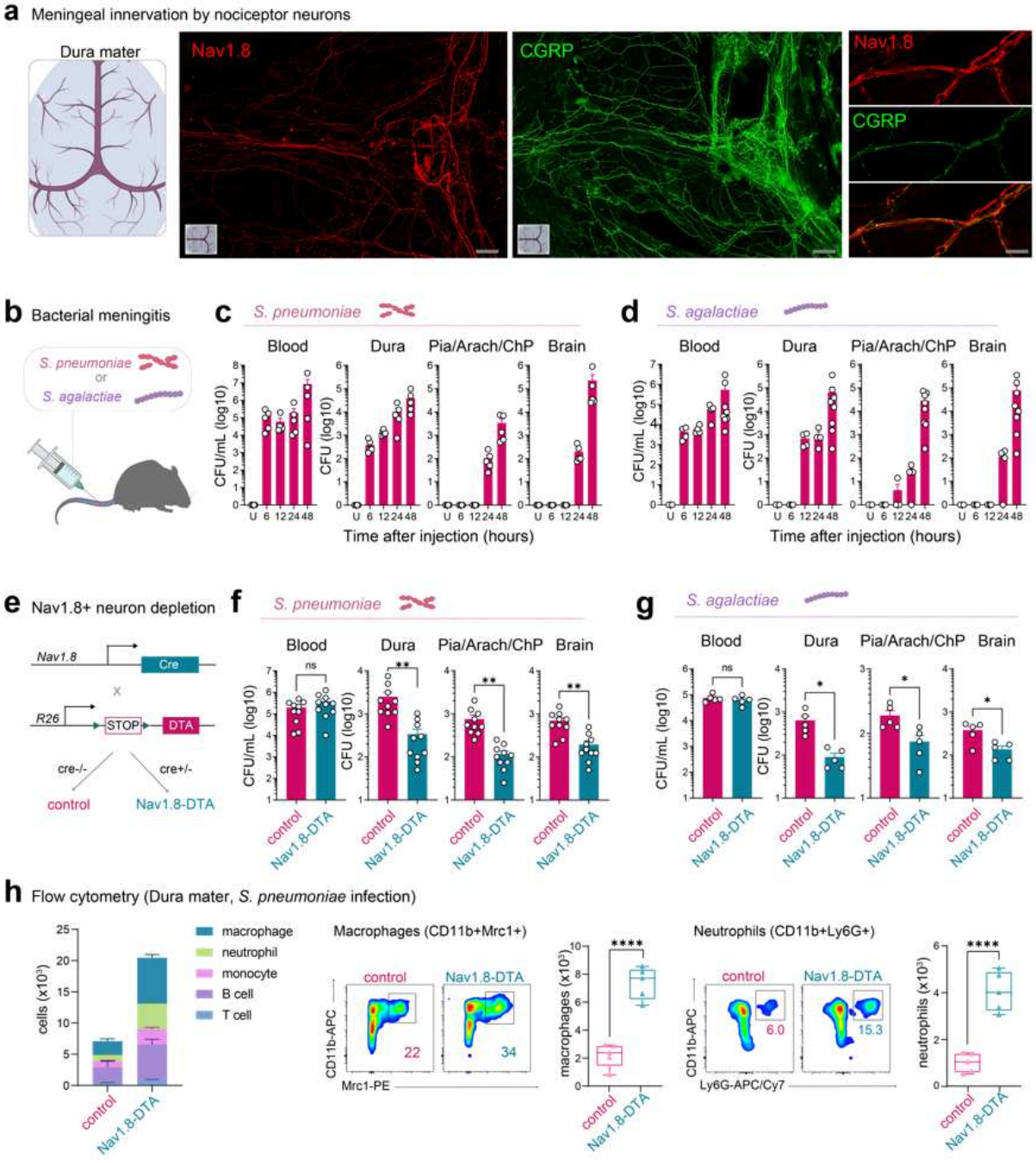
a Meningeal innervation by nociceptor neurons
Dura mater
Nav1.8
CGRP
b Bacterial meningitis
S. pneumoniae
or
S. agalactiae
c S. pneumoniae
d S. agalactiae
Blood
Dura
Pia/Arach/ChP
Brain
CFU/mL (log10)
CFU (log10)
U 6 12 24 48
Time after injection (hours)
e Nav1.8+ neuron depletion
Nav1.8
Cre
R26
STOP
DTA
cre-/-
cre+/-
control
Nav1.8-DTA
f S. pneumoniae
g S. agalactiae
ns
*
**
h Flow cytometry (Dura mater, S. pneumoniae infection)
cells (x10³)
macrophage
neutrophil
monocyte
B cell
T cell
Macrophages (CD11b+Mrc1+)
CD11b-APC
Mrc1-PE
22
34
macrophages (x10³)
****
Neutrophils (CD11b+Ly6G+)
Ly6G-APC/Cy7
6.0
15.3
neutrophils (x10³)

Fig. 1. Nociceptors regulate bacterial CNS invasion by *S. pneumoniae* and *S. agalactiae*. a, Whole-mount confocal images of mouse brain meninges (dura mater) showing the tissue innervation by Nav1.8+CGRP+ nociceptors. scale bar = 300 μm (low mag) and 15 μm (high mag). **b**, Scheme of hematogenous bacterial meningitis model in mice by intravenous (tail vein) injection of the human pathogens *S. pneumoniae* ($3x10^7$ c.f.u.) or *S. agalactiae* ($1x10^8$ c.f.u.). **c**, **d**, Bacterial load recovery from blood, Dura (Dura mater), Pia/Arach/ChP (Pia mater, Arachnoid mater, and Choroid Plexus), and Brain samples collected at different time points after injection with (**c**) *S. pneumoniae* or (**d**) *S. agalactiae* determined by quantitative culture (log c.f.u. plotted, n = 3-4 samples/time point). **e**, Genetic strategy to generate Nav1.8+ nociceptor deficient (Nav1.8-DTA) and control mice. **f**, **g**, Bacterial load in samples collected from Nav1.8-DTA and control mice 24h after injection of (**f**) *S. pneumoniae* or (**g**) *S. agalactiae* (n = 5-10/group). **h**, Flow cytometric quantification of meningeal immune cells of Nav1.8-DTA mice or control littermates 24h after *S. pneumoniae* injection. Left, combined numbers of immune cell subsets analyzed. Center, representative flow cytometry plots and quantification of meningeal macrophages (Cd11b+Mrc1+ gates). Right, representative flow cytometry plots and quantification of meningeal neutrophils (Cd11b+Ly6G+ gates). (n = 5/group). Statistical analysis: (**f**, **g**, **h**) Unpaired t tests. $*p < 0.05$, $**p < 0.01$, $****p < 0.0001$. ns = not significant. Mean ± SEM.

Figure 2

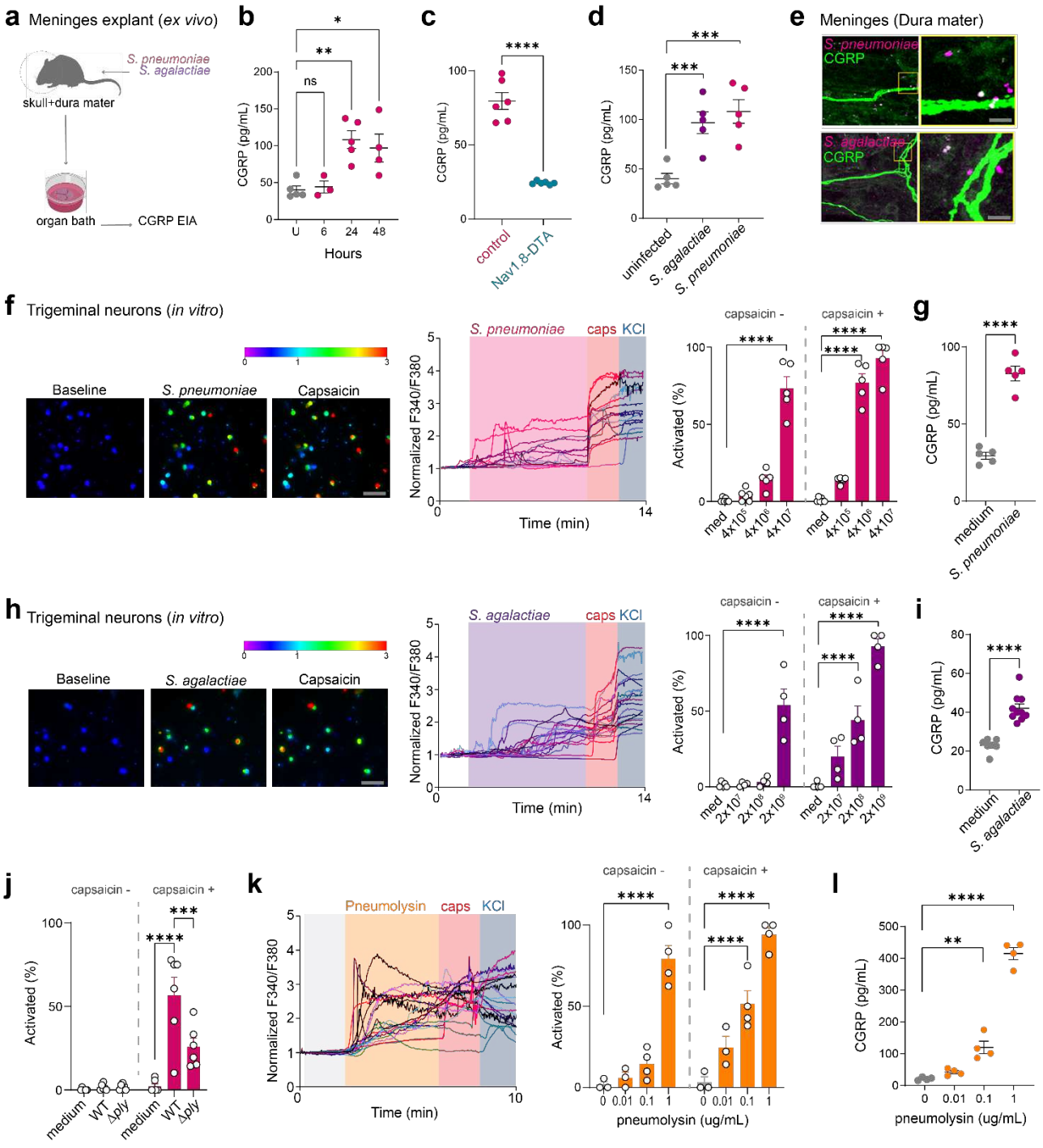
a Meninges explant (ex vivo)
S. pneumoniae
S. agalactiae
skull+dura mater
organ bath
CGRP EIA
b
CGRP (pg/mL)
Hours
U
6
24
48
ns
c
control
Nav1.8-DTA
d
uninfected
S. agalactiae
S. pneumoniae
e Meninges (Dura mater)
S. pneumoniae
CGRP
S. agalactiae
CGRP
f Trigeminal neurons (in vitro)
Baseline
S. pneumoniae
Capsaicin
Normalized F340/F380
Time (min)
capsaicin -
capsaicin +
Activated (%)
med
4x10⁵
4x10⁶
4x10⁷
g
medium
S. pneumoniae
h Trigeminal neurons (in vitro)
Baseline
S. agalactiae
Capsaicin
2x10⁷
2x10⁸
2x10⁹
i
medium
S. agalactiae
j
medium
WT
Δply
k
Pneumolysin
caps
KCl
pneumolysin (ug/mL)
l

Fig. 2. Bacteria activate nociceptors that release CGRP in the meninges. a-d, Measurement of CGRP levels released *ex vivo* from dural meninges explants. **a**, Scheme of meninges explant dissection from mice infected with *S. pneumoniae* ($3x10^7$ c.f.u.) or *S. agalactiae* ($1x10^8$ c.f.u.). **b**, time-course of CGRP release during bacterial meningitis induced by *S. pneumoniae* ($3x10^7$ c.f.u.). **c**, CGRP release from Nav1.8-DTA mice and control littermates 24h after injection of *S. pneumoniae* ($3x10^7$ c.f.u.). **d**, samples collected from uninfected mice and 24 h after injection of *S. pneumoniae* ($3x10^7$ c.f.u.) or *S. agalactiae* ($1x10^8$ c.f.u.). (n = 3-6/group). **e**, Whole-mount confocal images of mouse brain meninges (dura mater) showing the presence of bacteria nearby CGRP+ nociceptors 24h after injection of *S. pneumoniae* ($3x10^7$ c.f.u.) or *S. agalactiae* ($1x10^8$ c.f.u.). scale bar = 5 um. **f**, **g**, In vitro activation of trigeminal nociceptors by *S. pneumoniae*. **f**, Representative Fura-2 ratiometric fields (left) and calcium traces (center) of trigeminal ganglion neurons responding to *S. pneumoniae* ($4x10^7$ c.f.u.), capsaicin (1 µm), and/or KCl (40 mM). scale bar = 100 um. Right, proportions of capsaicin non-responsive (capsaicin−) and capsaicin responsive (capsaicin+) neurons that responded to *S. pneumoniae* ($4x10^5$ - $4x10^7$ c.f.u.) (n = 3–4 fields/condition). **g**, Concentration of CGRP in the supernatant of trigeminal neurons incubated with *S. pneumoniae* ($4x10^7$ c.f.u.) for 30 min. (n = 5/group). **h**, **i**, In vitro activation of trigeminal nociceptors by *S. agalactiae*. **h**, Representative Fura-2 ratiometric fields (left) and calcium traces (center) of trigeminal ganglion neurons responding to *S. agalactiae* ($4x10^9$ c.f.u.), capsaicin (1 µm), and/or KCl (40 mM). scale bar = 100 um. Right, proportions of capsaicin non-responsive (capsaicin−) and capsaicin responsive (capsaicin+) neurons that responded to *S. agalactiae* ($4x10^7$ - $4x10^9$ c.f.u.) (n = 3–4 fields/condition). **i**, Concentration of CGRP in the supernatant of trigeminal neurons incubated with *S. agalactiae* ($4x10^9$ c.f.u.) for 30 min. (n = 4-9/group). **j**, Pneumolysin-dependent activation of trigeminal nociceptors by *S. pneumoniae* ($4x10^6$ c.f.u.) (n = 6/group). **k**, **l**, Activation of trigeminal nociceptors by *S. pneumoniae* pore-forming toxin. **k**, Representative calcium traces (left) of trigeminal ganglion neurons responding to pneumolysin (1 ug/mL), capsaicin (1 µm), and/or KCl (40 mM). Right, proportions of capsaicin non-responsive (capsaicin−) and capsaicin

responsive (capsaicin+) neurons that responded to pneumolysin (0.01 – 1 ug/mL) (n = 3–4 fields/condition). **l**, Concentration of CGRP in the supernatant of trigeminal neurons stimulated with pneumolysin (0.01 – 1 ug/mL) for 30 min. (n = 4/group). Statistical analysis: (**a**, **c**, **e**, **g**, **i**, **j**, **k**) One-way ANOVA with Tukey post-tests. (**b**, **f**, **h**) Unpaired t tests. $*p < 0.05$, $**p < 0.01$, $***p < 0.001$, $****p < 0.0001$. ns = not significant. Mean ± SEM.

Figure 3

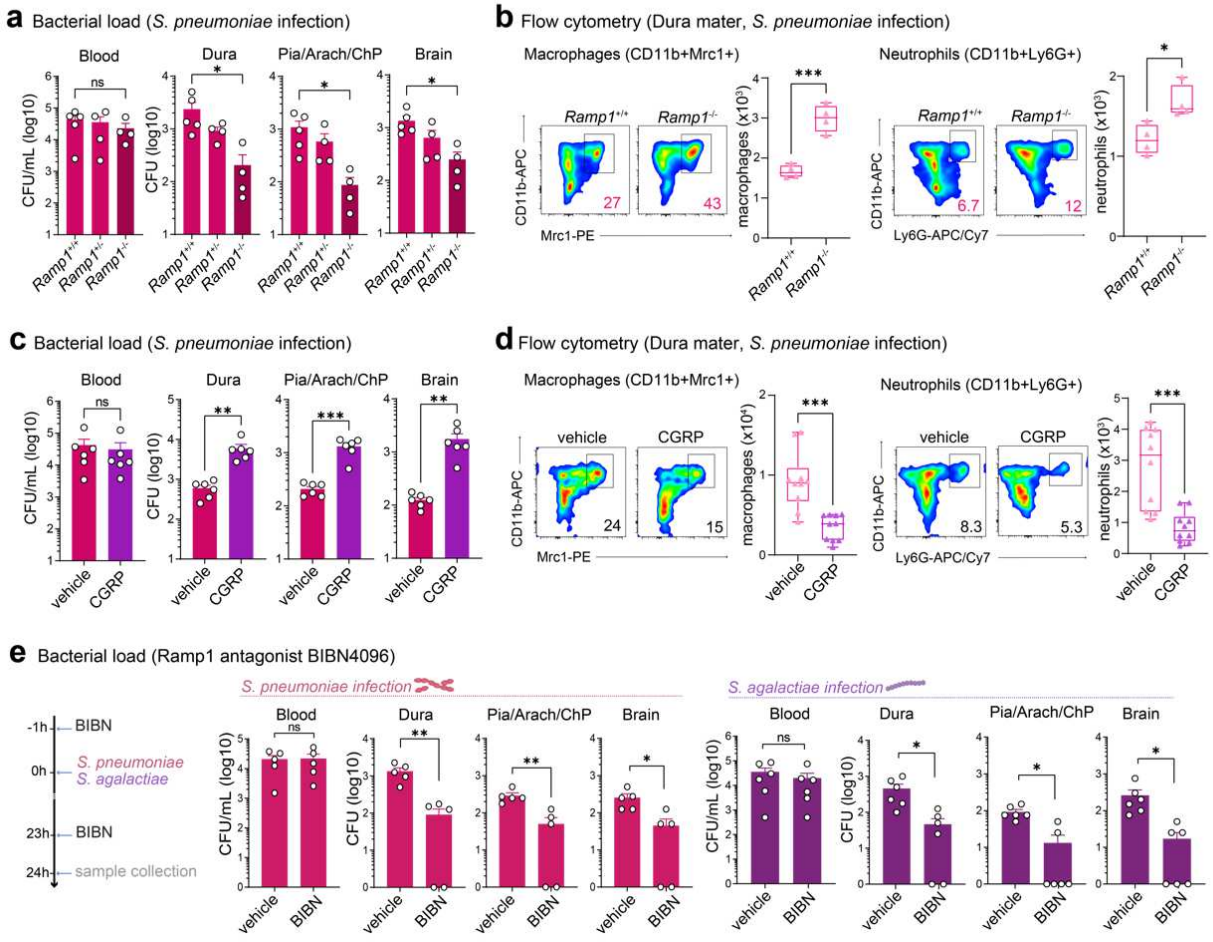
a Bacterial load (S. pneumoniae infection)
Blood
Dura
Pia/Arach/ChP
Brain
CFU/mL (log10)
CFU (log10)
ns
*
Ramp1+/+
Ramp1+/-
Ramp1-/-
b Flow cytometry (Dura mater, S. pneumoniae infection)
Macrophages (CD11b+Mrc1+)
Neutrophils (CD11b+Ly6G+)
CD11b-APC
Mrc1-PE
Ly6G-APC/Cy7
macrophages (x10³)
neutrophils (x10³)
27
43
6.7
12
***
c Bacterial load (S. pneumoniae infection)
**
***
vehicle
CGRP
d Flow cytometry (Dura mater, S. pneumoniae infection)
24
15
8.3
5.3
e Bacterial load (Ramp1 antagonist BIBN4096)
S. pneumoniae infection
S. agalactiae infection
-1h
BIBN
0h
S. pneumoniae
S. agalactiae
23h
BIBN
24h
sample collection
BIBN

Fig. 3. CGRP and RAMP1 signaling contribute to bacterial meningitis. a, b, Role of CGRP receptor Ramp1 in bacterial meningitis models. **a**, Bacterial load in samples collected from Ramp1 knockout ($Ramp1^{-/-}$) and control ($Ramp1^{+/-}$ and $Ramp1^{+/+}$) mice 24h after injection of *S. pneumoniae* (n = 4-5/group). **b**, Flow cytometric quantification of meningeal macrophages (Cd11b+Mrc1+ gates) and neutrophils (Cd11b+Ly6G+ gates) in Ramp1 knockout ($Ramp1^{-/-}$) and control ($Ramp1^{+/+}$) mice 24h after injection of *S. pneumoniae* (n = 4/group). **c, d,** Impact of CGRP injection on bacterial meningitis. **c**, Bacterial load in samples collected 24h after injection of *S. pneumoniae* in mice treated with CGRP (2 ug i.p., daily) or vehicle (saline) (n = 6/group). **d**, Flow cytometric quantification of meningeal macrophages (Cd11b+Mrc1+ gates) and neutrophils (Cd11b+Ly6G+ gates) 24h after injection of *S. pneumoniae* in mice treated with CGRP (2 ug i.p., daily) or vehicle (n = 10/group). **e,** Protective effects of treatment with a Ramp1 antagonist. Bacterial load in samples collected 24h after injection of *S. pneumoniae* (left, pink graphs) or *S. agalactiae* (right, purple graphs) in mice treated with Ramp1 antagonist (BIBN4096 300 ug/kg i.p., daily) or vehicle (n = 5-6/group). Statistical analysis: (**a**) One-way ANOVA with Tukey post-tests. (**b**, **c**, **d**, **e**) Unpaired t tests. $*p < 0.05$, $**p < 0.01$, $***p < 0.001$. ns = not significant. Mean ± SEM.

Figure 4

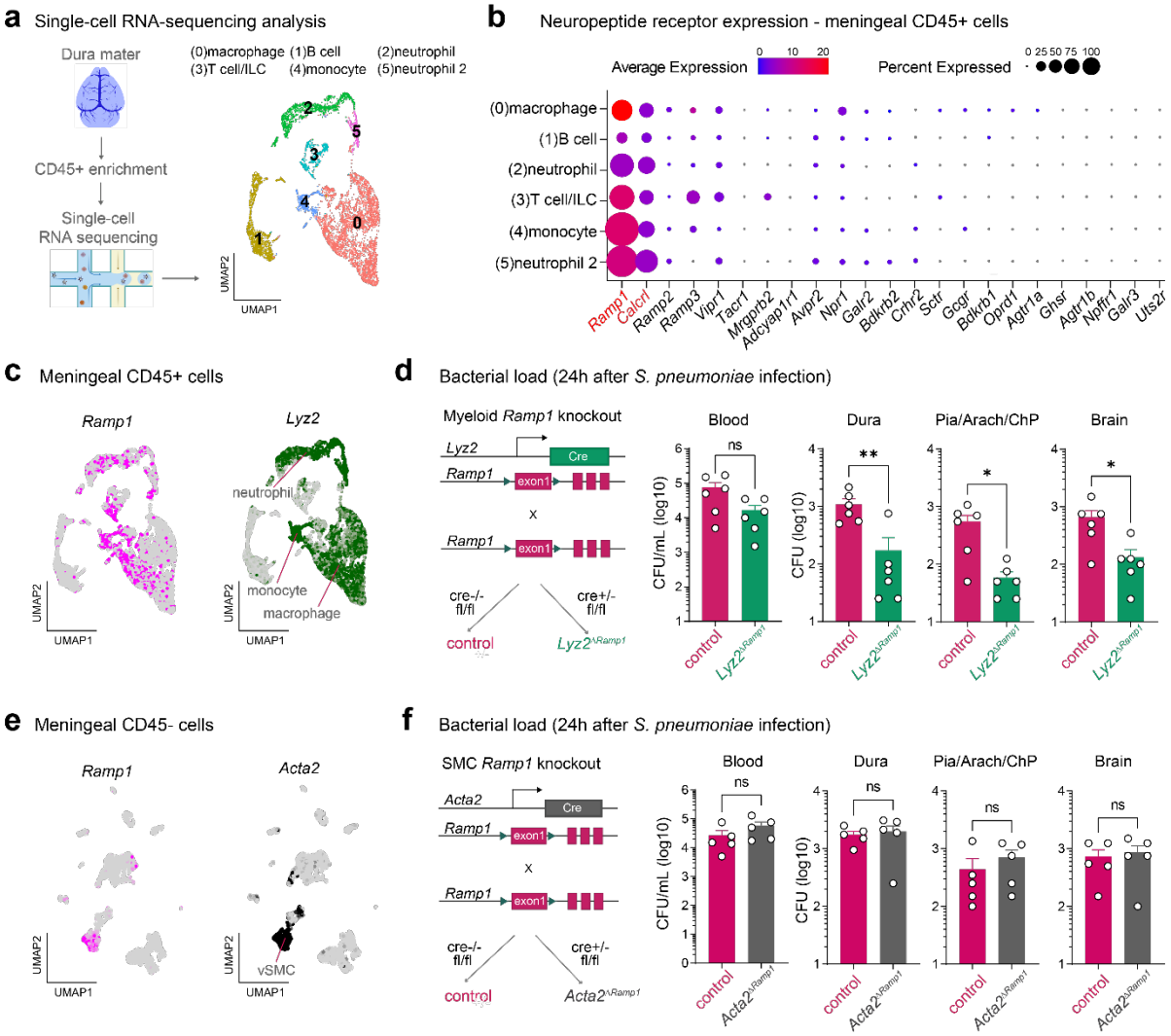
a
Single-cell RNA-sequencing analysis
Dura mater
CD45+ enrichment
Single-cell RNA sequencing
(0)macrophage (1)B cell (2)neutrophil
(3)T cell/ILC (4)monocyte (5)neutrophil 2
UMAP1
UMAP2
b
Neuropeptide receptor expression - meningeal CD45+ cells
Average Expression
Percent Expressed
(0)macrophage
(1)B cell
(2)neutrophil
(3)T cell/ILC
(4)monocyte
(5)neutrophil 2
Ramp1 Calcrl Ramp2 Ramp3 Vipr1 Tacr1 Mrgprb2 Adcyap1r1 Avpr2 Npr1 Galr2 Bdkrb2 Crhr2 Sctr Gcgr Bdkrb1 Oprd1 Agtr1a Ghsr Agtr1b Npffr1 Galr3 Uts2r
c
Meningeal CD45+ cells
Ramp1
Lyz2
neutrophil
monocyte
macrophage
d
Bacterial load (24h after S. pneumoniae infection)
Myeloid Ramp1 knockout
Lyz2
Cre
Ramp1
exon1
x
cre-/- fl/fl
cre+/- fl/fl
control
Lyz2ΔRamp1
Blood
Dura
Pia/Arach/ChP
Brain
CFU/mL (log10)
CFU (log10)
ns
**
*
e
Meningeal CD45- cells
Acta2
vSMC
f
Bacterial load (24h after S. pneumoniae infection)
SMC Ramp1 knockout
Acta2ΔRamp1

Fig. 4. Loss of myeloid *Ramp1* expression improves meningeal response against infection. a, **b,** Single-cell RNA-sequencing analysis of CD45-positive meningeal cells. **a**, Uniform Manifold Approximation and Projection (UMAP) visualizations of CD45-positive cell types in the meninges at baseline. **b**, Dot plots showing the average expression levels per cluster and the percentage of cells from each cluster expressing genes for neuropeptide receptors (n = 10 pooled meninges). **c**, UMAP visualization of expression for CGRP receptor gene *Ramp1* (left, pink) and myeloid marker gene *Lyz2* (right, green) in meningeal CD45-positive cells. **d**, Bacterial load in samples collected from myeloid-specific *Ramp1* knockout ($Lyz2^{\Delta Ramp1}$) and control mice 24h after injection of *S. pneumoniae* (n = 6/group). **e**, UMAP visualization of expression for CGRP receptor gene *Ramp1* (left, pink) and smooth muscle cell marker gene *Acta2* (right, dark gray) in meningeal CD45-positive cells. **f**, Bacterial load in samples collected from smooth muscle cell specific *Ramp1* knockout ($Acta2^{\Delta Ramp1}$) and control mice 24h after injection of *S. pneumoniae* (n = 5/group). Statistical analysis: (**d**, **f**) Unpaired t tests. $*p < 0.05$, $**p < 0.01$, $***p < 0.001$. ns = not significant. Mean ± SEM.

Figure 5

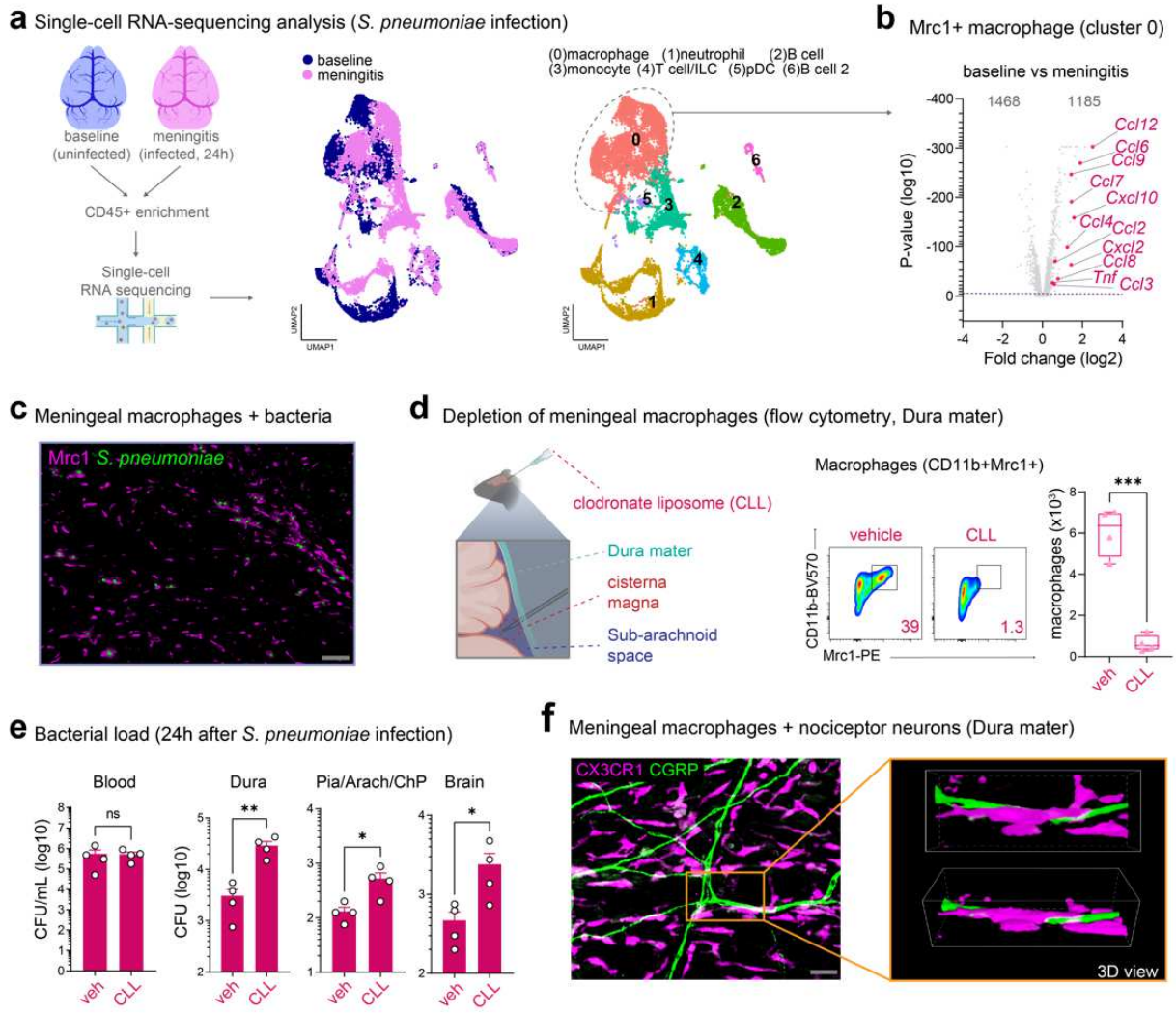
a Single-cell RNA-sequencing analysis (S. pneumoniae infection)
baseline (uninfected)
meningitis (infected, 24h)
CD45+ enrichment
Single-cell RNA sequencing
baseline
meningitis
UMAP2
UMAP1
(0)macrophage (1)neutrophil (2)B cell
(3)monocyte (4)T cell/ILC (5)pDC (6)B cell 2
b Mrc1+ macrophage (cluster 0)
baseline vs meningitis
1468
1185
Ccl12
Ccl6
Ccl9
Ccl7
Cxcl10
Ccl4
Ccl2
Cxcl2
Ccl8
Tnf
Ccl3
P-value (log10)
Fold change (log2)
c Meningeal macrophages + bacteria
Mrc1 S. pneumoniae
d Depletion of meningeal macrophages (flow cytometry, Dura mater)
clodronate liposome (CLL)
Dura mater
cisterna magna
Sub-arachnoid space
Macrophages (CD11b+Mrc1+)
vehicle
CLL
39
1.3
CD11b-BV570
Mrc1-PE
macrophages (x10³)
***
veh
CLL
e Bacterial load (24h after S. pneumoniae infection)
Blood
Dura
Pia/Arach/ChP
Brain
CFU/mL (log10)
CFU (log10)
ns
**
*
*
veh
CLL
f Meningeal macrophages + nociceptor neurons (Dura mater)
CX3CR1 CGRP
3D view

Fig. 5. Meningeal macrophages are required for protective host defense against *S. pneumoniae* infection. a-**b,** Single-cell RNA-sequencing analysis of meningeal immune responses to bacterial infection. **a**, Uniform Manifold Approximation and Projection (UMAP) visualizations of CD45-positive cell types in the meninges at baseline and 24h after injection of *S. pneumoniae* (meningitis). **b**, Volcano plot from scRNA-seq analysis showing genes that are differentially expressed in the cluster of Mrc1+ macrophages in response to infection (baseline vs meningitis) highlighting the upregulation of chemotaxis-related genes (n = 10 pooled meninges/group). **c**, Whole-mount confocal images of mouse meninges (dura mater) showing meningeal macrophages (Mrc1+ cells) associated with *S. pneumoniae* 24h post injection of CMTPX-labeled bacteria. Scale bar = 25 um. **d**, Depletion of meningeal Mrc1+ macrophages by intracisternal injection of clodronate liposomes (CLL) 3 days before infections. Flow cytometric quantification of meningeal macrophages (Cd11b+Mrc1+ gates) 24h after injection of *S. pneumoniae* in mice treated with CLL (5 μL) or vehicle. **e**, Bacterial load in samples collected 24h after injection of *S. pneumoniae* in mice treated with CLL (5 μL) or vehicle. (n = 4/group). **f**, Whole-mount confocal images of mouse brain meninges (dura mater) showing the presence of macrophages (CX3CR1+ cells) near CGRP+ nociceptors. Scale bar = 10 um. Statistical analysis: (**b**) Wilcoxon rank-sum test, dashed purple line = $p < 0.01$. (**d**, **e**) Unpaired t tests. $*p < 0.05$, $**p < 0.01$, $***p < 0.001$. ns = not significant. Mean ± SEM.

Figure 6

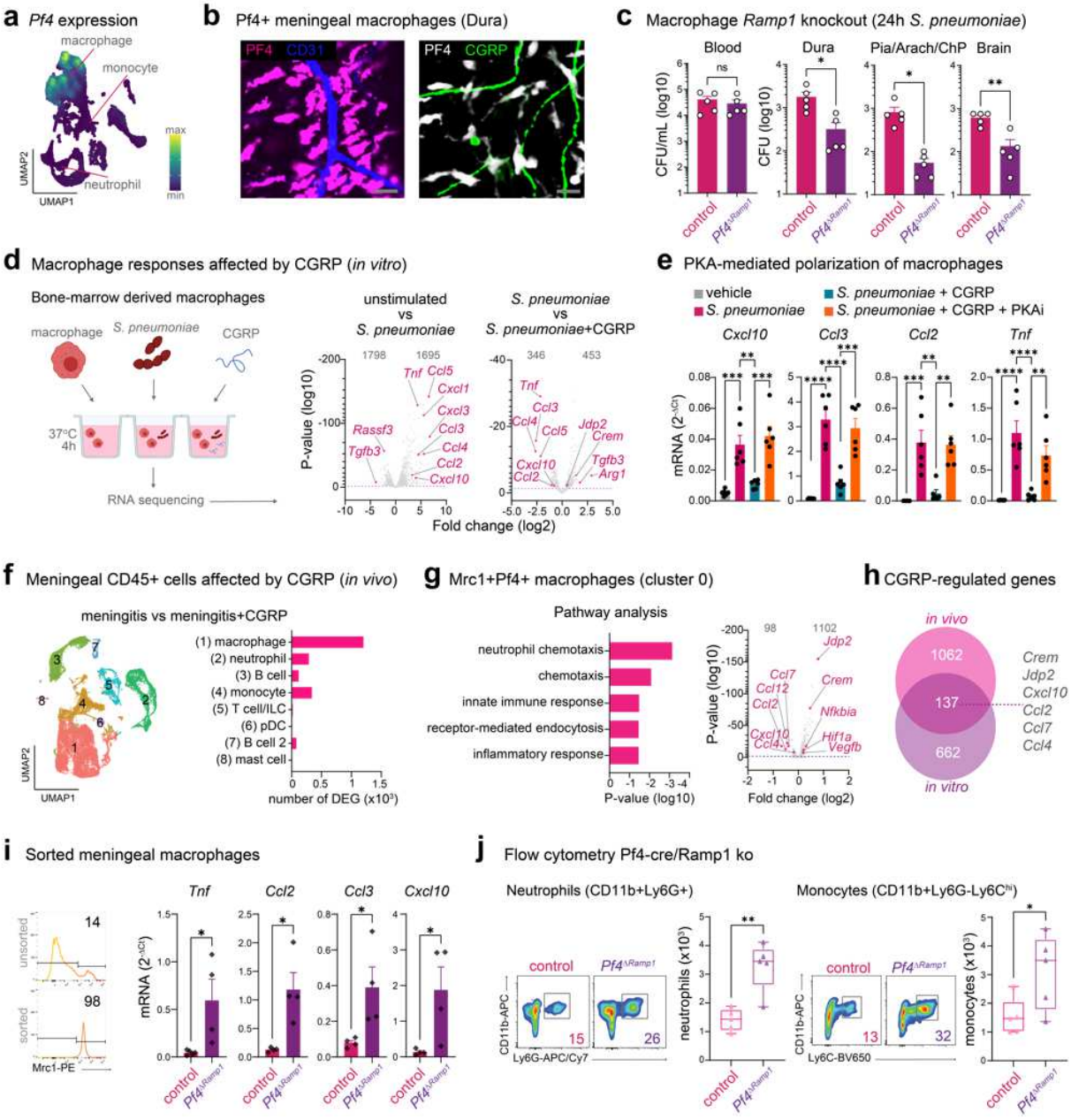
a Pf4 expression
macrophage
monocyte
neutrophil
UMAP1
UMAP2
max
min
b Pf4+ meningeal macrophages (Dura)
PF4 CD31
PF4 CGRP
c Macrophage Ramp1 knockout (24h S. pneumoniae)
Blood
Dura
Pia/Arach/ChP
Brain
CFU/mL (log10)
CFU (log10)
ns
control
Pf4ΔRamp1
d Macrophage responses affected by CGRP (in vitro)
Bone-marrow derived macrophages
macrophage
S. pneumoniae
CGRP
37°C
4h
RNA sequencing
unstimulated vs S. pneumoniae
S. pneumoniae vs S. pneumoniae+CGRP
P-value (log10)
Fold change (log2)
Tnf
Ccl5
Cxcl1
Cxcl3
Ccl3
Ccl4
Ccl2
Cxcl10
Rassf3
Tgfb3
Jdp2
Crem
Arg1
e PKA-mediated polarization of macrophages
vehicle
S. pneumoniae
S. pneumoniae + CGRP
S. pneumoniae + CGRP + PKAi
Cxcl10
Ccl3
Ccl2
Tnf
mRNA (2^-ΔCt)
f Meningeal CD45+ cells affected by CGRP (in vivo)
meningitis vs meningitis+CGRP
(1) macrophage
(2) neutrophil
(3) B cell
(4) monocyte
(5) T cell/ILC
(6) pDC
(7) B cell 2
(8) mast cell
number of DEG (x10³)
g Mrc1+Pf4+ macrophages (cluster 0)
Pathway analysis
neutrophil chemotaxis
chemotaxis
innate immune response
receptor-mediated endocytosis
inflammatory response
P-value (log10)
Fold change (log2)
Jdp2
Ccl7
Ccl12
Ccl2
Crem
Nfkbia
Cxcl10
Ccl4
Hif1a
Vegfb
h CGRP-regulated genes
in vivo
in vitro
1062
137
662
Crem
Jdp2
Cxcl10
Ccl2
Ccl7
Ccl4
i Sorted meningeal macrophages
unsorted
sorted
Mrc1-PE
14
98
Tnf
Ccl2
Ccl3
Cxcl10
mRNA (2^-ΔCt)
j Flow cytometry Pf4-cre/Ramp1 ko
Neutrophils (CD11b+Ly6G+)
Monocytes (CD11b+Ly6G-Ly6C^hi)
CD11b-APC
Ly6G-APC/Cy7
Ly6C-BV650
neutrophils (x10³)
monocytes (x10³)
15
26
13
32

Fig. 6. CGRP suppresses macrophage-mediated meningeal immunity. a, **b**, *Pf4* is specifically expressed by meningeal macrophages. **a**, UMAP visualization of Pf4 expression in the cluster of meningeal macrophages (cluster #0). **b**, Whole-mount confocal images of mouse brain meninges (dura mater) showing the presence of PF4+ macrophages near blood vessels (CD31) and CGRP+ nociceptors. **c**, Bacterial load in samples collected from macrophage specific *Ramp1* knockout ($Pf4^{\Delta Ramp1}$) and control mice 24h after injection of *S. pneumoniae* (n = 5/group). **d**, **e**, In vitro assay using bone marrow-derived macrophages (BMDM). **d**, Volcano plots from RNA sequencing analysis showing genes that are differentially expressed in macrophage cultures. Left, transcriptional changes in response to *S. pneumoniae* (unstimulated vs *S. pneumoniae*), highlighting the upregulation of chemotaxis-related genes. Right, list of genes that are affected when macrophages are incubated with *S. pneumoniae* in the presence of CGRP (*S. pneumoniae* vs *S. pneumoniae*+CGRP) highlighting the downregulation of chemotaxis-related genes (n = 4/group). **e**, Expression of chemotaxis-related genes in macrophages exposed to *S. pneumoniae*, CGRP, and PKA inhibitor (PKAi) determined by qPCR. Results are presented relative to housekeeping gene beta actin expression (n = 6/group). **f**, **g**, Single-cell RNA-sequencing analysis of meningeal immune responses to bacterial infection and CGRP treatment. **f**, Left, Uniform Manifold Approximation and Projection (UMAP) visualizations of CD45-positive cell types in the meninges collected from uninfected mice, infected with *S. pneumoniae*, and/or treated with CGRP. Right, number of genes that were affected by CGRP treatment in each immune cell population during infection (meningitis vs meningitis+CGRP). **g**, Annotated GO biological processes and volcano plot of genes differentially expressed by the cluster of macrophages in infected mice treated with CGRP when compared to meningeal macrophages from infected, vehicle-treated mice (meningitis vs meningitis+CGRP), highlighting the downregulation of chemotaxis-related genes (n = 10 pooled meninges/group). **h**, Venn diagram highlighting the overlap of genes affected by CGRP *in vitro* and *in vivo.* **i**, Expression of chemotaxis-related genes by qPCR in macrophages sorted from the meninges of macrophage-specific

Ramp1 knockout (*Pf4*$^{\Delta Ramp1}$) and control mice 24h after injection of *S. pneumoniae.* Results are presented relative to housekeeping gene beta actin expression (n = 4/group). **j**, Flow cytometric quantification of neutrophils (Cd11b+Ly6G+ gates) and monocytes (Cd11b+Ly6G-Ly6C^{hi} gates) in the meninges of macrophage-specific *Ramp1* knockout (*Pf4*$^{\Delta Ramp1}$) and control mice 24h after injection of *S. pneumoniae* (n = 5/group). Statistical analysis: (**d**, **g**) Wilcoxon rank-sum test, dashed purple line = $p < 0.01$. (**c**, **i**, **j**) Unpaired t tests. (**e**) One-way ANOVA with Tukey post-tests. $*p < 0.05$, $**p < 0.01$, $***p < 0.001$, $****p < 0.0001$. ns = not significant. Mean ± SEM.

Extended Data Figure 1

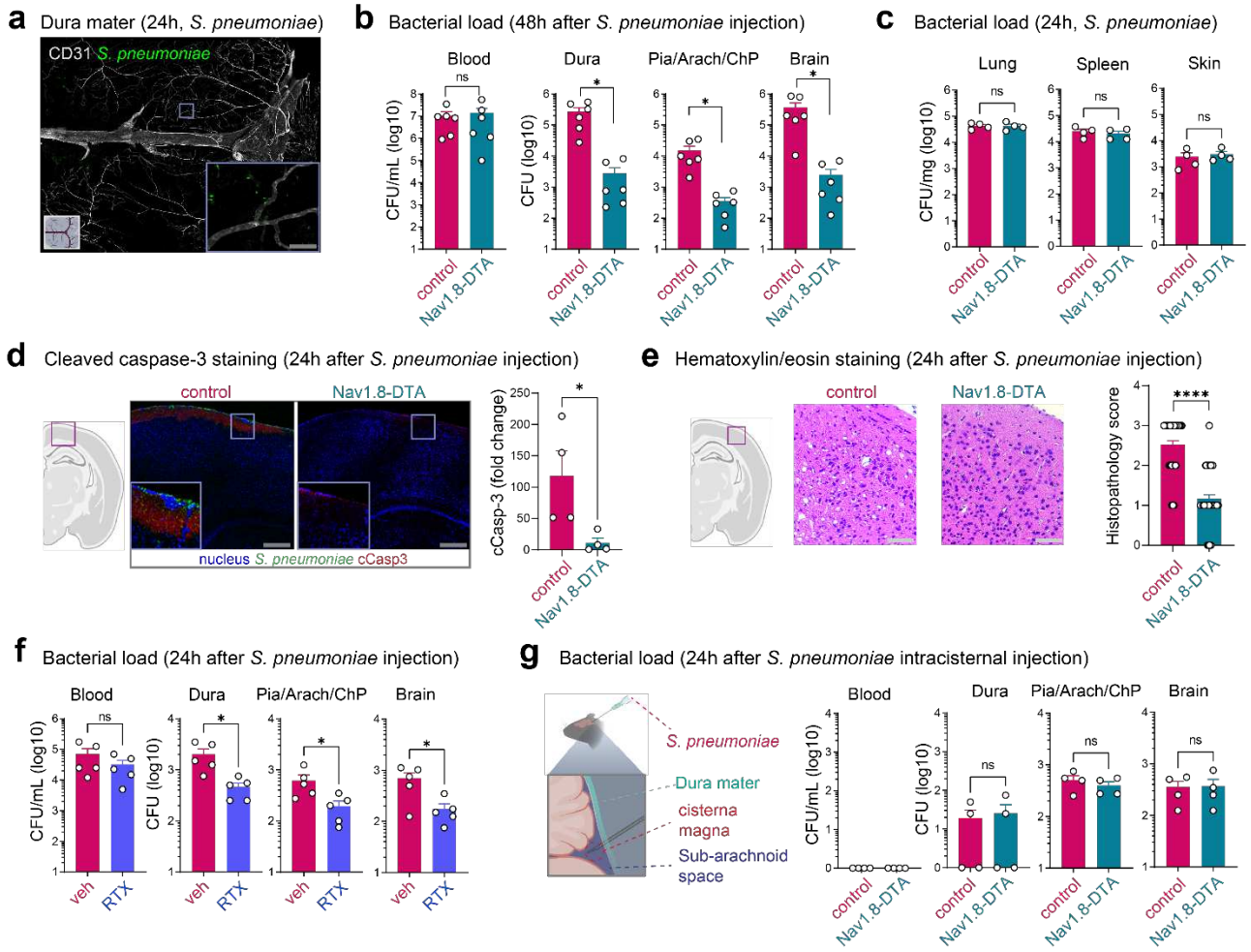

Extended Fig. 1. Nociceptors suppress meninges-mediated protection of CNS to infection. a, Whole-mount confocal images of mouse meninges (dura mater) showing extravascular localization of *S. pneumoniae* 24h post-injection of CMTPX-labeled bacteria. Scale bar = 100 um. **b**, Bacterial load in samples collected from Nav1.8-DTA and control mice 48h after injection of *S. pneumoniae* (n = 6/group). **c**, Bacterial load in samples collected from Nav1.8-DTA and control mice 24h after injection of *S. pneumoniae* (n = 4/group). **d**, Quantification of cleaved caspase-3 staining in brain samples collected from Nav1.8-DTA and control mice 24h after injection of CMTPX-labeled *S. pneumoniae.* Results are presented as fold-change relative to cCasp-3 staining of brain samples from uninfected mice (n=3-4/group). Scale bar = 200 um. **e**, Histopathology score of brain samples collected from Nav1.8-DTA and control mice 24h after injection of *S. pneumoniae.* (n=12 fields/sample, 4 samples/group). Scale bar = 50 um. **f**, Bacterial load in samples collected 24h after injection of *S. pneumoniae* from mice treated with resiniferatoxin (RTX) or vehicle (n = 5/group). **g**, Bacterial load in samples collected from Nav1.8-DTA and control mice 24h after intracisternal injection of *S. pneumoniae* (n = 4/group). Statistical analysis: (**b**, **c**, **d**, **e**, **f**, **g**) Unpaired t tests. $*p < 0.05$, $****p < 0.0001$. ns = not significant. Mean ± SEM.

Extended Data Figure 2

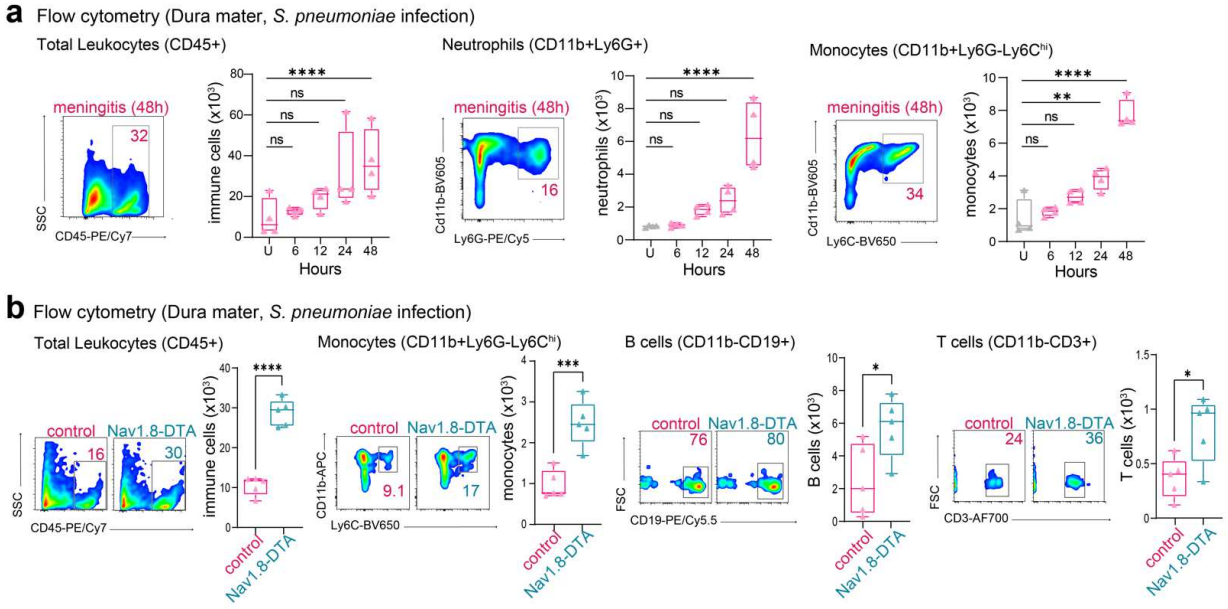

Extended Fig 2. Nociceptors regulate meningeal immunity against bacterial infection. a, Representative flow cytometry plots and quantification of total leukocytes (CD45+ gate), neutrophils (CD11b+Ly6G+ gates), and monocytes (CD11b+Ly6G-Ly6C^{hi} gates) in the meninges at different time points after injection of *S. pneumoniae* (n = 4/group). **b**, Representative flow cytometry plots and quantification of total leukocytes (CD45+ gate), monocytes (CD11b+Ly6G-Ly6C^{hi} gates), B cells (CD11b-CD19+ gates), and T cells (CD11b-CD3+) in the meninges of Nav1.8-DTA mice or control littermates 24h after *S. pneumoniae* injection (n = 5/group). Statistical analysis: (**d**, **g**) Wilcoxon rank-sum test, dashed purple line = $p < 0.01$. (**c**, **i**, **j**) Unpaired t tests. (**e**) One-way ANOVA with Tukey post-tests. $*p < 0.05$, $**p < 0.01$, $***p < 0.001$, $****p < 0.0001$. ns = not significant. Mean ± SEM. Statistical analysis: (**b**) Unpaired t tests. (**a**) One-way ANOVA with Tukey post-tests. $*p < 0.05$, $**p < 0.01$, $***p < 0.001$, $****p < 0.0001$. ns = not significant. Mean ± SEM.

Extended Data Figure 3

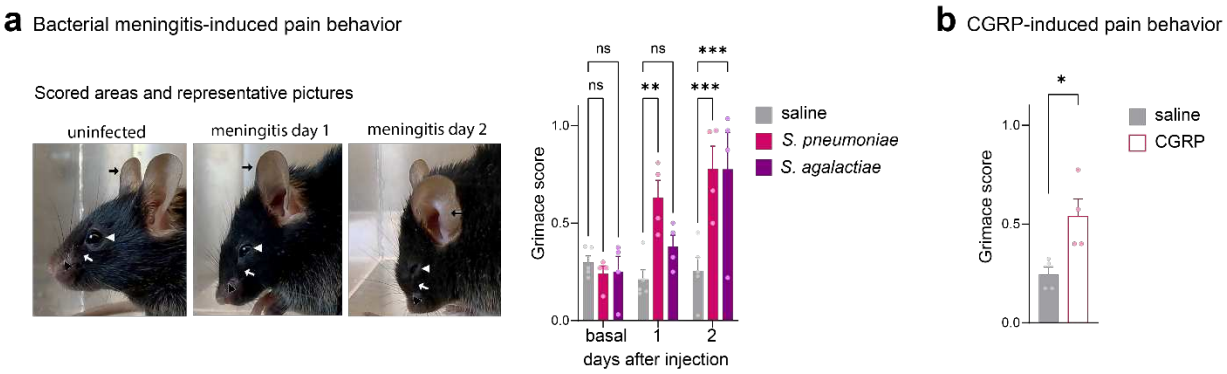

Extended Fig. 3. Bacterial meningitis causes pain behavior. a, Representative pictures and grimace scores of mice at baseline (uninfected), 1 day, and 2 days after injection of *S. pneumoniae*, *S. agalactiae*, or vehicle (n = 4-5/group). **b**, Grimace scores of mice injected with CGRP (2 ug, i.p.) or vehicle (n = 4/group). Statistical analysis: (**b**) Unpaired t tests. (**a**) One-way ANOVA with Tukey post-tests. $*p < 0.05$, $**p < 0.01$, $***p < 0.001$. ns = not significant. Mean ± SEM.

Extended Data Figure 4

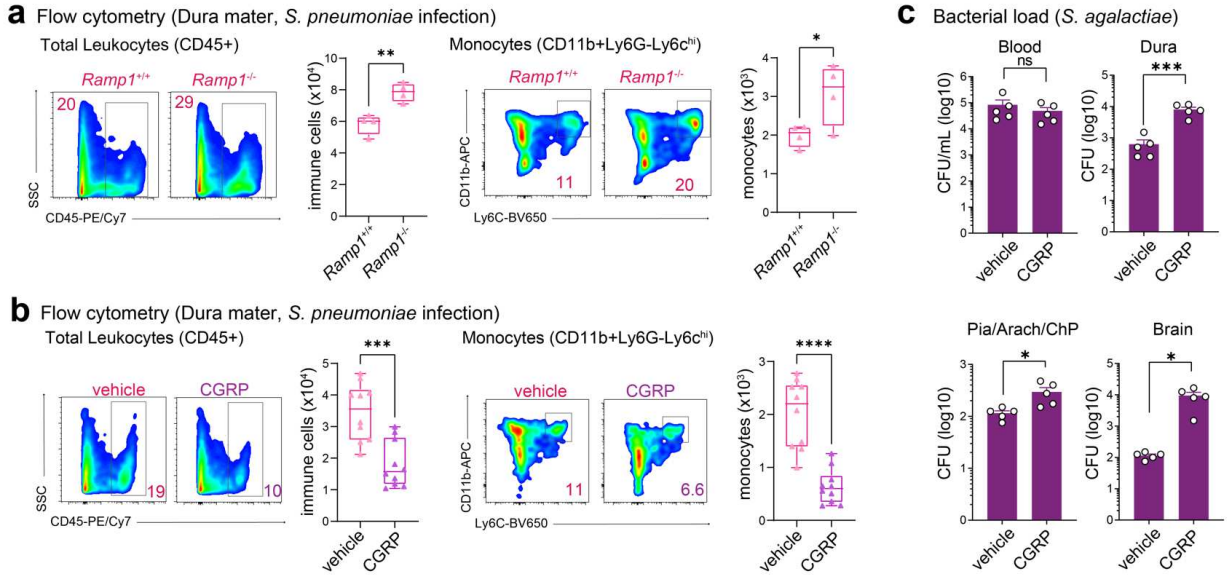

Extended Fig. 4. CGRP and RAMP1 signaling impair host response against bacterial meningitis. a, Representative flow cytometry plots and quantification of total leukocytes (CD45+ gate) and monocytes (CD11b+Ly6G-Ly6C^{hi} gates) in the meninges of *Ramp1* knockout (*Ramp1*$^{-/-}$) and control (*Ramp1*$^{+/+}$) mice 24h after *S. pneumoniae* injection (n = 4/group). **b**, Representative flow cytometry plots and quantification of total leukocytes (CD45+ gate) and monocytes (CD11b+Ly6G-Ly6C^{hi} gates) 24h after *S. pneumoniae* injection in the meninges of mice treated with CGRP or vehicle (n = 10/group). **c**, Bacterial load 24h after injection of *S. agalactiae* in samples from mice treated with CGRP or vehicle (n = 5/group). Statistical analysis: (**a**, **b**, **c**) Unpaired t tests. $*p < 0.05$, $**p < 0.01$, $***p < 0.001$, $****p < 0.0001$. ns = not significant. Mean ± SEM.

Extended Data Figure 5

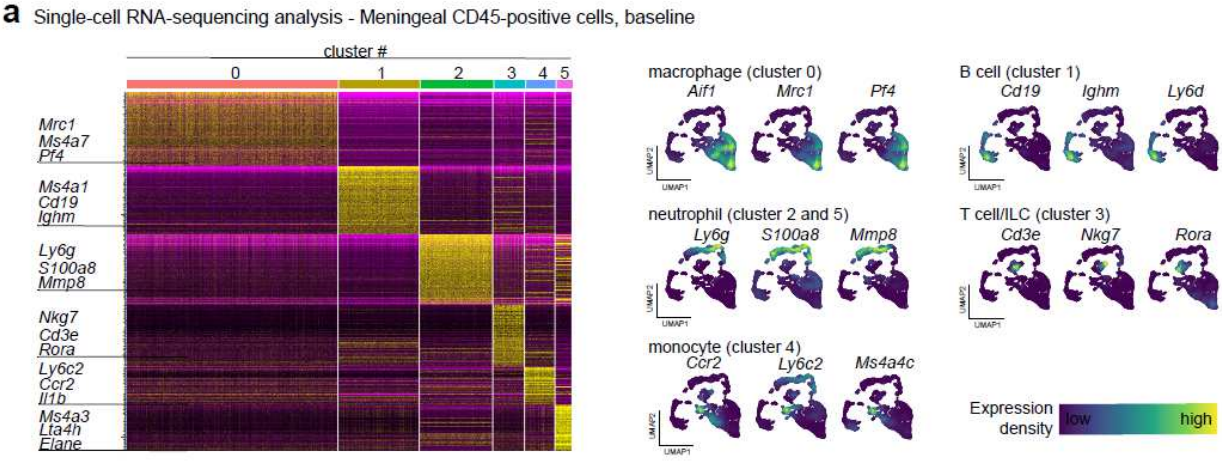

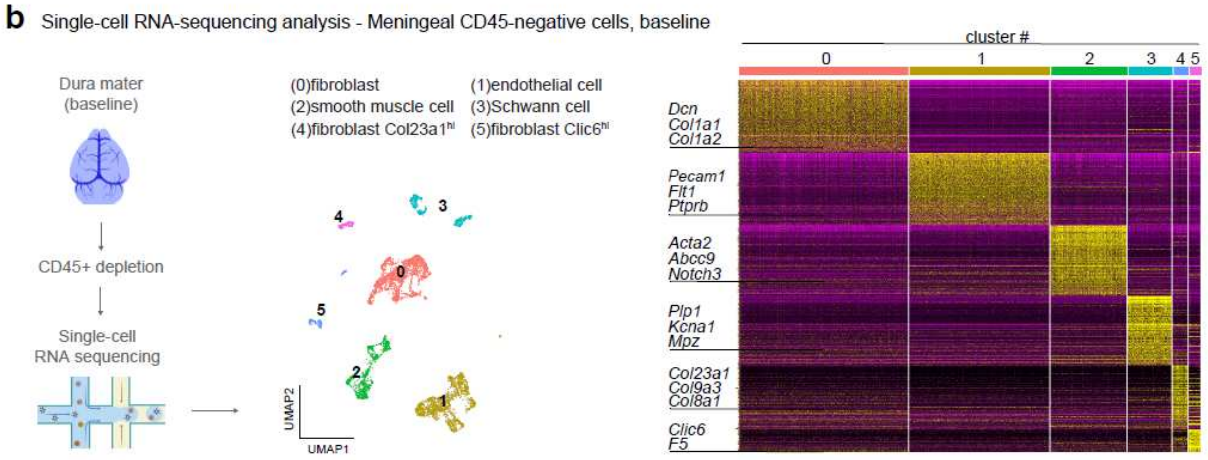

Extended Fig. 5. Single-cell RNA-sequencing analysis of meningeal cells. a, Single-cell RNA-sequencing analysis of meningeal immune cells (CD45-positive cells). Left, heatmap showing normalized expression of 100 top cluster marker genes in meningeal immune cells of the meninges, with key marker genes highlighted. Right, UMAP visualization of the expression of key marker genes for each immune cell cluster (n = 10 pooled meninges). **b**, Single-cell RNA-sequencing analysis of meningeal nonimmune cells (CD45-negative cells). Left, Uniform Manifold Approximation and Projection (UMAP) visualizations of CD45-negative cell types in the meninges at baseline. Right, heatmap showing normalized expression of 100 top cluster marker genes in nonimmune cells of the meninges, with key marker genes highlighted (n = 10 pooled meninges).

Extended Data Figure 6

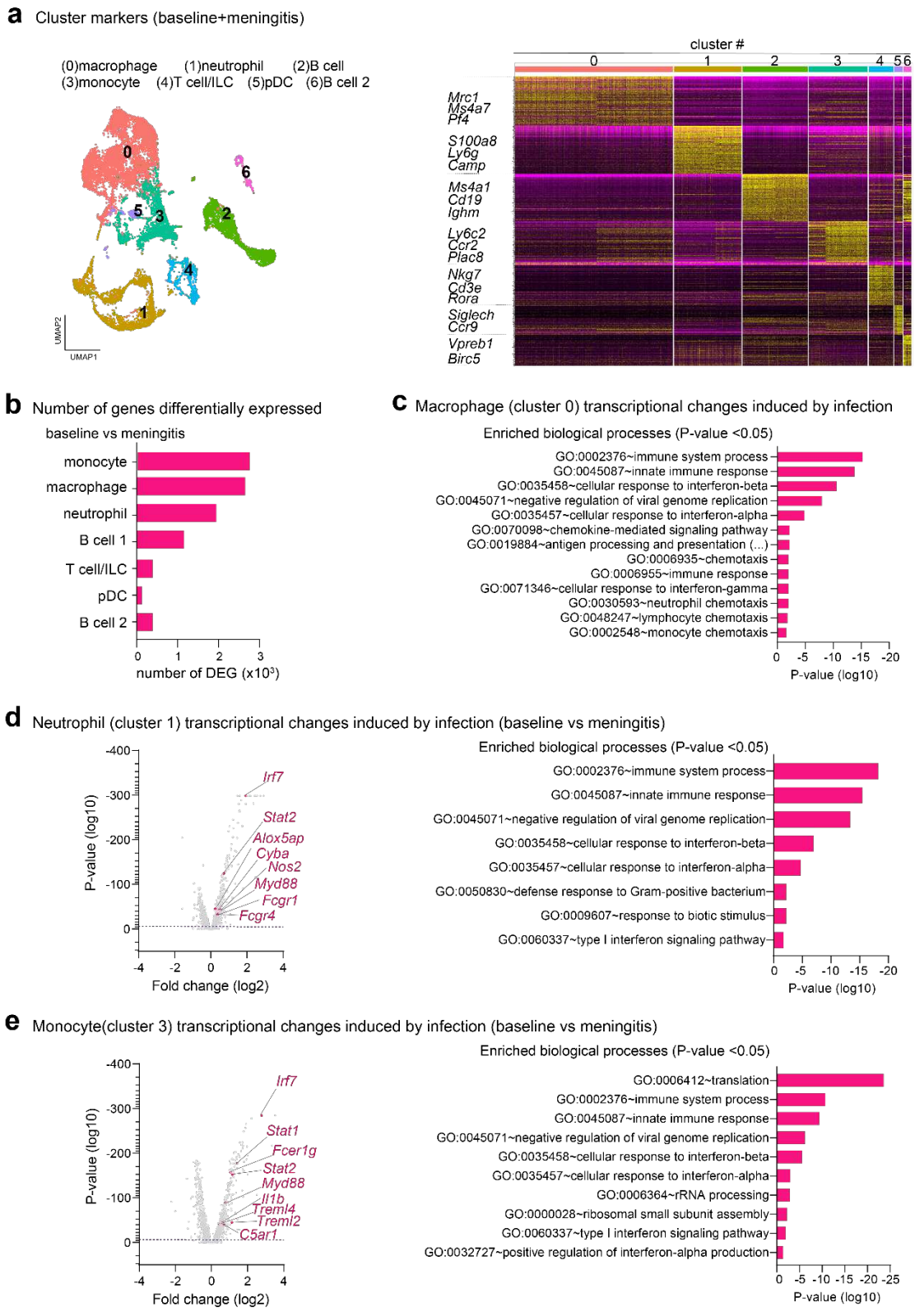

Extended Fig. 6. Transcriptional responses of meningeal immune cells to bacterial meningitis. a, Single-cell RNA-sequencing analysis of meningeal immune responses to bacterial infection. Left, Uniform Manifold Approximation and Projection (UMAP) visualizations of CD45-positive cell types in the meninges at baseline and 24h after injection of *S. pneumoniae* (meningitis). Right, heatmap showing normalized expression of 100 top cluster marker genes with key immune marker genes highlighted. **b**, Number of genes that were differentially expressed in each immune cell population during infection (baseline vs meningitis). **c**, Annotated GO biological processes of genes differentially expressed by the cluster of macrophages in response to infection (baseline vs meningitis), highlighting the enrichment of processes related to chemotaxis. **d**, Annotated GO biological processes and volcano plot of genes differentially expressed by the cluster of neutrophils in response to infection (baseline vs meningitis), highlighting upregulation of processes and genes related to antimicrobial activity. **e**, Annotated GO biological processes and volcano plot of genes differentially expressed by the cluster of monocytes in response to infection (baseline vs meningitis). (n = 10 pooled meninges/group). Statistical analysis: (**c**, **d**, **e**) Fisher's Exact score (enriched biological processes) and Wilcoxon rank-sum test (volcano plots of DEG), dashed purple line = $p < 0.01$.

Extended Data Figure 7

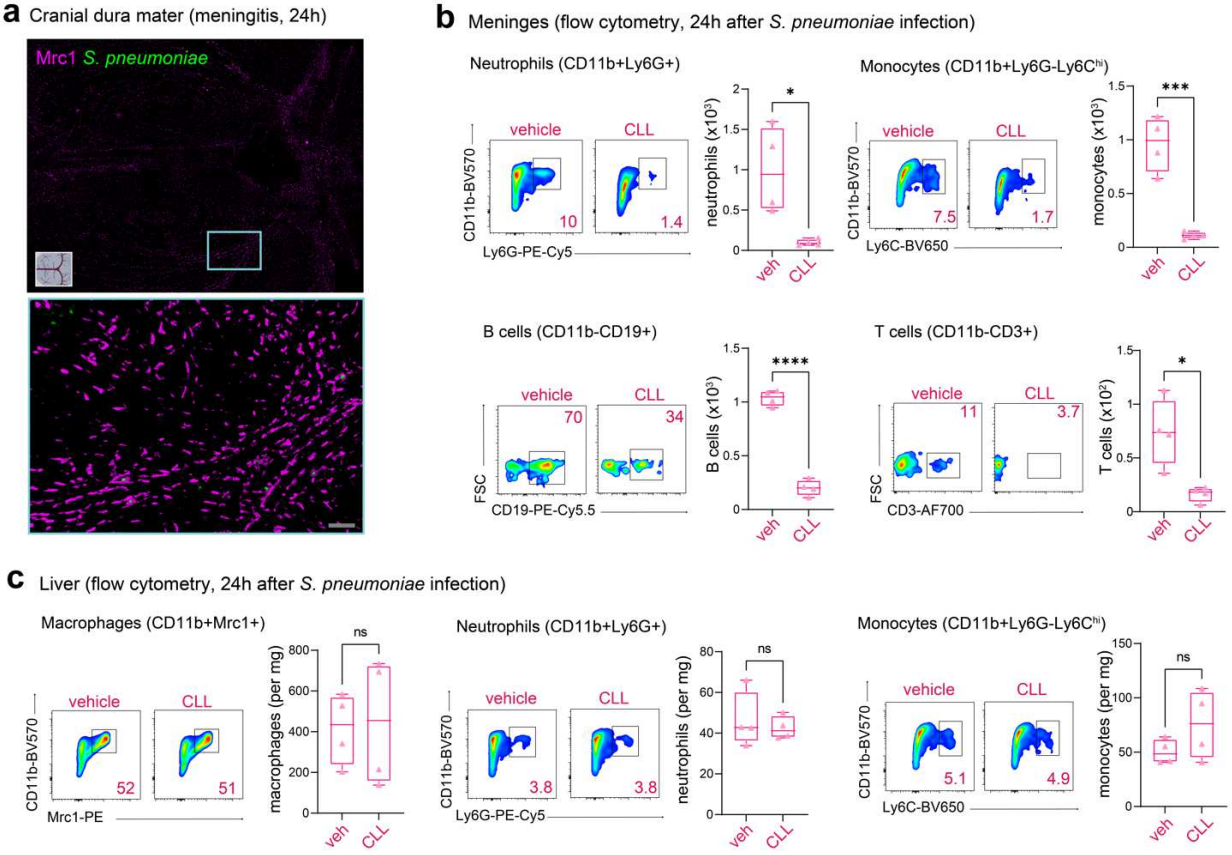

Extended Fig. 7. Meningeal macrophages engulf bacteria and regulate immune responses against bacterial invasion. a, Whole-mount confocal images of mouse meninges (dura mater) showing meningeal macrophages (Mrc1+ cells) associated with *S. pneumoniae* 24h post-injection of CMTPX-labeled bacteria. Scale bar = 50 um. **b**, **c**, Tissue-specific impact of depletion of meningeal Mrc1+ macrophages by intracisternal injection of clodronate liposomes (CLL). **b**, Representative flow panels and quantification of neutrophils (CD11b+Ly6G+ gates), monocytes (CD11b+Ly6G-Ly6C^{hi} gates), B cells (CD11b-CD19+ gates), and T cells (CD11b-CD3+ gates) 24h after injection of *S. pneumoniae* in mice treated with CLL (5 μL) or vehicle. **c**, Representative flow panels and quantification of macrophages (CD11b+Mrc1+ gates), neutrophils (CD11b+Ly6G+ gates), and monocytes (Cd11b+Ly6G-Ly6C^{hi} gates) in the liver of mice treated with CLL (5 μL) or vehicle. (n = 4/group). Statistical analysis: (**b**, **c**) Unpaired t tests. $*p < 0.05$, $***p < 0.001$, $****p < 0.0001$. ns = not significant. Mean ± SEM.

Extended Data Figure 8

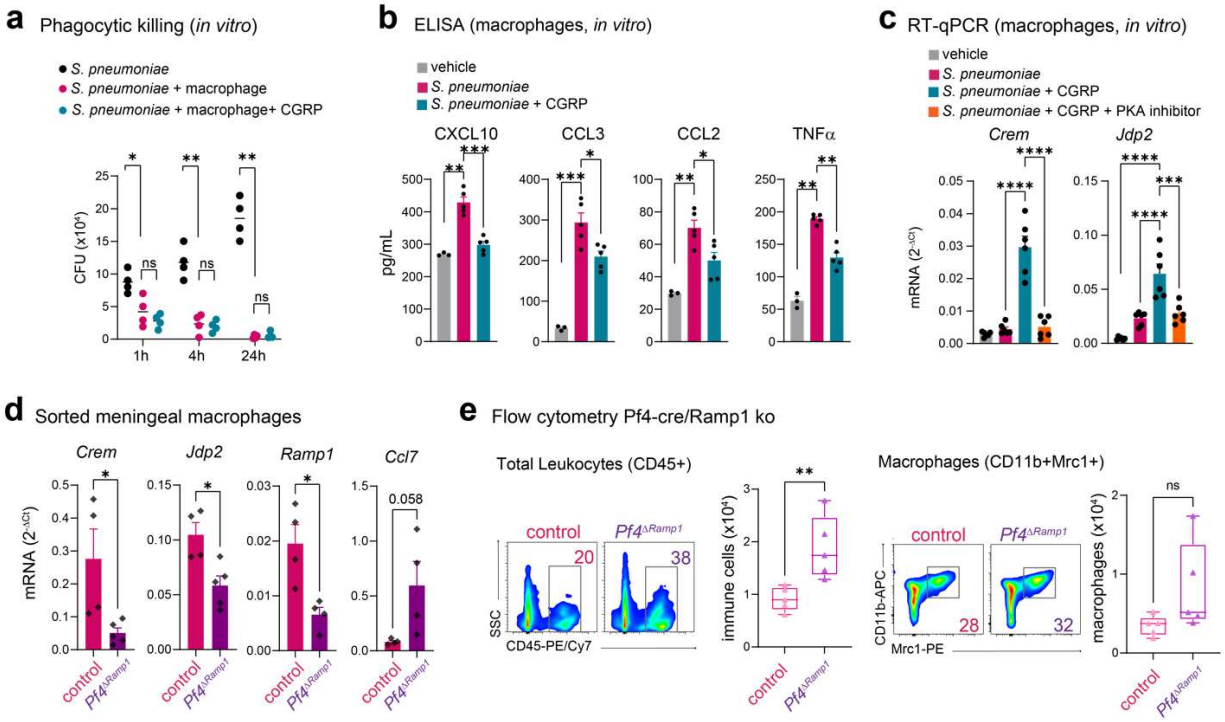

Extended Fig. 8. CGRP and RAMP1 polarization of macrophage responses. a, Phagocytic killing assay showing the amount of *S. pneumoniae* recovered at different time points of incubation with mouse macrophages (BMDM) in presence of CGRP or vehicle (n = 4/group). **b**, Concentration of chemotaxis-related mediators in the supernatant of macrophages after 24h of incubation with *S. pneumoniae* in the presence of CGRP or vehicle (n = 3-5/group). **c**, Quantification of *Crem* and *Jdp2* mRNA determined by qPCR in macrophages after 4h incubation with *S. pneumoniae* in the presence of CGRP, PKA inhibitor (PKAi), or vehicle. Results are presented relative to housekeeping gene beta actin expression (n = 6/group). **d**, Quantification of *Crem*, *Jdp2*, *Ramp1*, and *Ccl7* mRNA determined by qPCR in macrophages sorted from the meninges of macrophage specific *Ramp1* knockout ($Pf4^{\Delta Ramp1}$) and control mice 24h after injection of *S. pneumoniae.* Results are presented relative to housekeeping gene beta actin expression (n = 4/group). **e**, Flow cytometric quantification of total leukocytes (CD45+ gate) and macrophages (Cd11b+Mrc1+ gates) in the meninges of macrophage specific *Ramp1* knockout ($Pf4^{\Delta Ramp1}$) and control mice 24h after injection of *S. pneumoniae* (n = 5/group). Statistical analysis: (**a**, **b**, **c**) One-way ANOVA with Tukey post-tests. (**d**, **e**) Unpaired t tests. $*p < 0.05$, $**p < 0.01$, $***p < 0.001$, $****p < 0.0001$. ns = not significant. Mean ± SEM.

Extended Data Figure 9

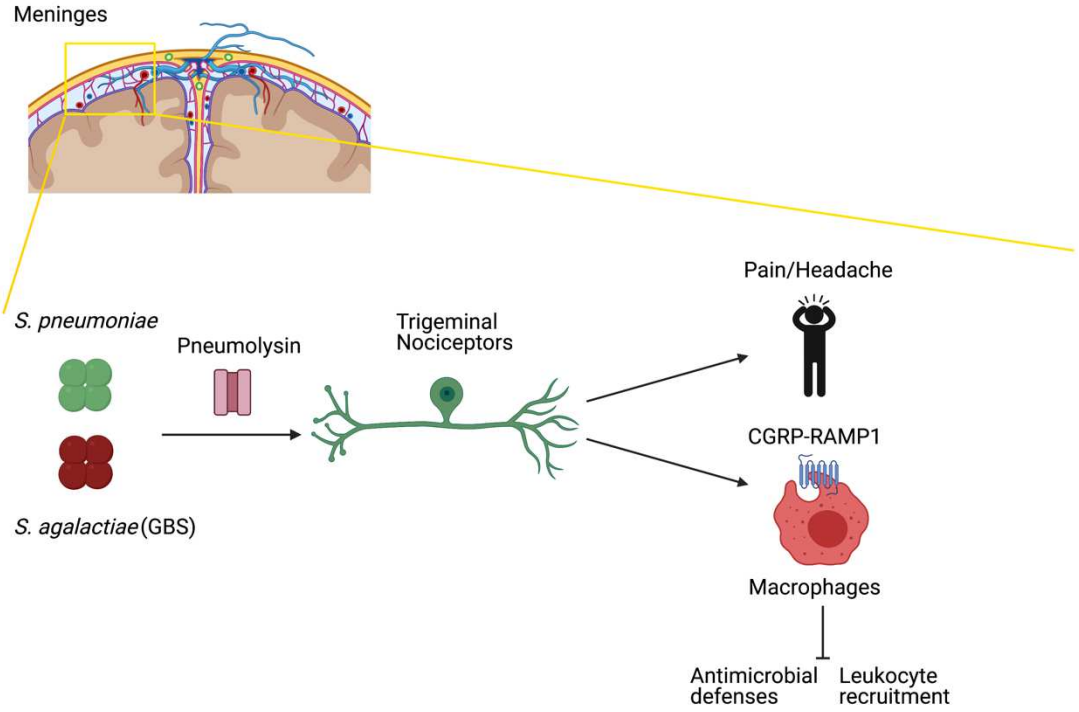

Extended Fig. 9. Neuroimmune and microbial interactions in bacterial meningitis revealed in the study. In this study, we find that the bacterial pathogens *S. pneumoniae* and *S. agalactiae* (Group B Streptococcus) activate trigeminal nociceptors that innervate the meninges to induce pain and neuroimmune signaling during bacterial meningitis in mice. For *S. pneumoniae*, neuronal activation is mediated by pneumolysin (PLY). Following nociceptor activation, the neuropeptide CGRP is released in the dural meninges, which acts through the CGRP receptor RAMP1 on meningeal macrophages to polarize transcriptional responses, downregulating the expression of chemokines that results in suppression of leukocyte recruitment and antimicrobial defenses. Blockade of CGRP signaling or ablation of nociceptors enhances host defenses against bacterial meningitis.

Acknowledgments

We thank Richard Malley for providing *S. pneumoniae* strains used in this study and for valuable advice. We thank Jason Buenrostro and Rojesh Shrestha for advice on computational analysis and other collaborations. We thank Michael R. Wessels, Darren E. Higgins, Maria Lehtinin, Huixin Xu, Thiago Mattar Cunha, and members of the Chiu lab helpful discussions. We thank Nicole C El-Ali, Nathan Weeks, and Harvard University Bauer Core Facility for technical support. We thank Samantha Choi, Stacie Lin, Nicole Marie Gilette, Karina Lezgiyeva, Sébastien John Sannajust, Emily Erhard, Olivia Clancy, and Aleksandr Prystupa for technical help and data analysis. We thank Abigail Frey for manuscript feedback. We thank Jennifer L. Gibbs for mentorship. This work was supported by funding from National Institutes of Health (NIH) R01AI130019 and R01DK127257 to I.M.C.; 2R01NS078263 and 5R01NS115972 to D.L.; P50MH112491 to the Conte Center; R01NS116716 to K.S.D; T32GM007753 to D.V.N.; Burroughs Wellcome Fund and Chan-Zuckerberg Initiative to I.M.C.; K.H. was supported by Harvard Medical School Undergraduate Immunology Summer Program.

Author contributions

Conceptualization: F.A.P.-R. and I.M.C.; Resources and Bacterial Strains: D.L., K.S.D., and B.S.; Experimentation and Acquisition of Data: F.A.P.-R., L.D., O.E., S.C.N., G.W., K.H.; Data Analysis: F.A.P.-R., D.N., O.E., K.H., A.J.W.; Writing the manuscript: F.A.P.-R. and I.M.C., with inputs from all authors; Funding Acquisition: I.M.C.

Competing interests

I.M.C. is on advisory boards for GSK pharmaceuticals and LIMM therapeutics, and his lab receives funding from Allergan Pharmaceuticals. B.S. is on advisory boards of Neurmora and Annexon Biosciences. None of these relationships influenced the work performed in this study.

Additional information

Correspondence and requests for materials should be addressed to I.M.C. (isaac_chiu@hms.harvard.edu)

Methods

Bacterial strains and culture

All procedures related to pathogenic bacteria were approved by the Committee on Microbiological Safety of Harvard Medical School and conducted under Biosafety Level 2 protocols and guidelines. The *Streptococcus pneumoniae* clinical isolate WU2 (serotype 3), the *S. pneumoniae* isogenic pneumolysin mutant strain WU2-PLA[1], and *Streptococcus agalactiae* clinical isolate COH1 (serotype III)[2] were used in this study. *S. pneumoniae* and *S. agalactiae* were grown in Tryptic Soy Broth (Sigma) and Todd-Hewitt Broth (Sigma), respectively, supplemented with 0.5% yeast extract (Sigma). Bacteria were grown at 37°C with 5% CO_2 to mid-log phase, and growth was evaluated by monitoring OD_{600}. Frozen stocks of bacteria in 20% glycerol (Sigma) were prepared and kept at −80°C until use.

Animals

All experiments and procedures using mice were approved by the Institutional Animal Care and Use Committee (IACUC) at Harvard Medical School and were conducted in accordance with National Institutes of Health (NIH) animal research guidelines. Mice were bred and housed in individually ventilated micro isolator cages within a full barrier, specific pathogen-free animal facility at Harvard Medical School under a 12 h light/dark cycle with ad libitum access to food and water. C57BL/6 mice were purchased from Jackson Laboratories (Bar Harbor, ME) or Charles River (Worcester, MA). C57BL/6-Tg (Pf4-icre)Q3Rsko/J, B6.FVB-Tg(Acta2-cre)1Rkl/J, B6.129P2-*Lyz2*$^{tm1(cre)Ifo}$/J, B6.129P2-*Gt(ROSA)26Sor*$^{tm1(DTA)Lky}$/J, CX3CR1-GFP, and B6.129S2(Cg)-*Ramp1*$^{tm1.1Tsuj}$/WkinJ mice were purchased from Jackson Laboratories. Calca-GFP were provided by V. Kuchroo (Harvard Medical School). *Nav1.8-Cre* mice (Abrahamsen et al., 2008) were provided by J. Wood (University College London). Nav1.8-mCitrine mice were provided by D Levy (BIDMC/Harvard Medical School). *Ramp1*$^{fl/fl}$ (C57BL/6N-*Ramp1*$^{tm1c(EUCOMM)Wtsi}$/H) mice were purchased

from MRC Harwell Institute (Oxfordshire, UK). *Calca* or B6.129S2(Cg)-*Ramp1*$^{tm1.1Tsuj}$/WkinJ heterozygous mice were bred together to produce wild-type and knockout littermates. *Nav1.8-Cre* heterozygous (+/−) mice were bred with B6.129P2-*Gt(ROSA)26Sor*$^{tm1(DTA)Lky}$/J homozygous (+/+) mice to generate nociceptor-ablated Nav1.8-DTA (*Nav1.8-Cre*$^{+/-}$;*Dta*$^{+/-}$) mice and control littermates (*Nav1.8-Cre*$^{-/-}$;*Dta*$^{+/-}$). For conditional knockout experiments, Pf4$^{\Delta Ramp1}$ (C57BL/6-Tg(Pf4-icre)Q3Rsko/J$^{+/-}$; *Ramp1*$^{fl/fl}$), Lyz2$^{\Delta Ramp1}$ (B6.129P2-*Lyz2*$^{tm1(cre)Ifo}$/J$^{+/-}$; *Ramp1*$^{fl/fl}$), and Acta2$^{\Delta Ramp1}$ (B6.FVB-Tg(Acta2-cre)1Rkl/J$^{+/-}$; *Ramp1*$^{fl/fl}$) mice were bred to *Ramp1*$^{fl/fl}$ mice to generate mice with specific depletion of Ramp1 in meningeal macrophages (Pf4$^{\Delta Ramp1}$), myeloid cells (Lyz2$^{\Delta Ramp1}$), vascular smooth muscle cells (Acta2$^{\Delta Ramp1}$), and control littermates (cre$^{-/-}$; *Ramp1*$^{fl/fl}$). Both male and female age-matched mice from 8 to 14 weeks of age were used for all experiments in this study.

Hematogenous bacterial meningitis

Bacteria strains were grown to mid-log phase as described in the section *Bacterial strains and culture*. Bacteria were centrifuged at 5,000*g* for 15 min, resuspended in saline solution to a final concentration of 3x10^8 c.f.u./mL for *S. pneumoniae* and 1x10^9 c.f.u./mL for *S. agalactiae*. The bacterial suspension was kept on ice until use. A total volume of 100 µL of inoculum containing *S. pneumoniae* (3x10^7 c.f.u.) or *S. agalactiae* (1x10^8 c.f.u.) was injected into the tail vein (intravenous injection) of 8-14 weeks old mice using a 0.5 cc syringe fitted with a 31-gauge needle (BD Biosciences). An aliquot of the final suspension was used to confirm the concentration of bacteria in the inoculum by plating serial dilutions on blood agar plates.

Bacterial load recovery analysis

Mice were deeply anesthetized with intraperitoneal injection of tribromoethanol solution (Avertin, 500 mg/kg) and perfused transcardially with saline solution. Blood was sampled right before perfusion. Other tissue samples (meninges, choroid plexus, brain, liver, skin) were dissected and weighed. Tissues were then transferred to 2 mL eppendorf tubes containing 5 mm stainless steel beads (QIAGEN) and 1 mL of ice-cold sterile saline. Tissues were homogenized in TissueLyser II (QIAGEN) for 10 min at 30 Hz. To determine bacterial load recovery, serial dilutions were made and plated on TSA plates with 5% Sheep Blood plates (BD Biosciences). The plates were incubated overnight at 37°C with 5% CO2 and the number of c.f.u. in each plate determined.

Ablation of nociceptors by resiniferatoxin (RTX) injection

RTX (Sigma-Aldrich) was used to deplete TRPV1-positive nociceptors as previously described[3]. Male and female 4-week-old C57BL/6 mice were lightly anesthetized by inhalation of isoflurane (Patterson Veterinary) 3% in oxygen using a precision vaporizer. Mice received subcutaneous injections of escalating doses of RTX (30 µg/kg, 70 µg/kg, 100 µg/kg) or vehicle control (PBS with 1.2% DMSO and 0.06% Tween-80) on three consecutive days. Mice were used for experiments four weeks after the injections.

Isolation and culture of trigeminal neurons

The trigeminal ganglia were dissected immediately after euthanasia by CO_2 inhalation. Trigeminal cells were enzymatically dissociated in 2 mL of HEPES-buffered saline (Sigma) containing collagenase A (1 mg/kg, Sigma) and dispase II (2.4 U/mL, Roche Applied Sciences) for 40 min at 37°C. Cells were centrifuged for 5 min at 300*g* at and resuspended in 800 µL of DMEM/10% FBS containing DNase I (150U/mL, Thermo Fisher). Trigeminal cells were dissociated by gently pipetting with decreasing tip diameters to create

single-cell suspensions. Cells were resuspended in 2 mL of neurobasal medium (Life Technologies), and the cell suspension was added to the top of a 10% BSA gradient in neurobasal medium. Cells were centrifuged at 260*g* for 10 min, the supernatant containing cell debris was discarded, and the resulting pellet was resuspended in neurobasal medium for cell counting and plating. For calcium imaging experiments, 2,000 trigeminal neurons were plated onto each culture dish previously coated with laminin and incubated overnight in neurobasal-A medium supplemented with 50 ng/mL nerve growth factor (Thermo Fisher). For CGRP release experiments, 5,000 trigeminal neurons were transferred to each well of a flat bottom 96-wells plate previously coated with laminin and incubated with neurobasal-A medium plus 50 ng/mL nerve growth factor (Thermo Fisher) and cytosine arabinoside (10 µM, Sigma) for 6 days.

Intracellular calcium levels and CGRP release in cultures of trigeminal neurons

Cultures of mouse trigeminal neurons were prepared as described in *Isolation and culture of trigeminal neurons.* For calcium measurements, neurons were loaded with the calcium indicator Fura-2 AM (5 µM, Thermo Fisher) for 30 min at 37°C, washed twice with Krebs-Ringer solution (Boston BioProducts), and immediately imaged using an Eclipse Ti-S/L100 inverted microscope (Nikon) and Zyla sCMOS camera. Excitation of Fura-2-AM was induced with ultraviolet light source (Lambda XL lamp, Sutter Instrument) at 340 nm and 380 nm wavelengths. The 340/380 ratiometric images were acquired and analyzed using NIS-elements software (Nikon). After recording the baseline calcium levels for 2 min, cells were stimulated with *S. pneumoniae* ($4x10^5$ - $4x10^7$ c.f.u./mL), *S. agalactiae* ($2x10^7$ - $2x10^9$ c.f.u./mL), or pneumolysin (0.01-1 µg/mL), followed by capsaicin (1 µM) and KCl (40 mM). An increase of 15% or more from baseline calcium levels was considered a positive response to a ligand. Cells that did not respond to the positive controls (capsaicin and KCl) were excluded from the quantification. For CGRP release assay, neurons were incubated with *S. pneumoniae* ($4x10^7$ c.f.u./mL), *S. agalactiae* ($2x10^9$ c.f.u./mL), or pneumolysin (0.01-1

μg/mL) for 30 min (37°C, 5% CO_2). After incubation, the supernatant was collected and used to quantify the concentration of CGRP using an Enzyme Linked Immunosorbent kit (Cayman Chemical) according to manufacturer`s instructions.

Isolation and culture of bone marrow-derived macrophages

Mouse bone marrow-derived macrophages (BMDM) were obtained as previously described[4] with minor modifications. Progenitor cells were harvested from the bone marrow of femur and tibia and cultured in DMEM supplemented with 10% FBS, 1% penicillin-streptomycin solution (15140122 Gibco), and macrophage-colony stimulating factor (20 ng/mL, 15140122 PeproTech) for 8 days (37 °C, 5% CO_2). Culture media was replaced with fresh supplemented DMEM at day 4. Fully differentiated macrophages (>90% of cells CD11b+F4/80+ determined by flow cytometry) were harvested at day 8 and immediately used for experiments.

Phagocytic killing assay

Cultures of mouse macrophages (BMDM) were prepared as described in *Isolation and culture of bone marrow-derived macrophages*. *S. pneumoniae* ($5x10^5$ c.f.u. per well) was co-incubated with mouse macrophages ($5x10^5$ cells per well) in DMEM supplemented with 10% of mouse serum for 1h-24h (37°C, 5% CO_2) with gentle shaking (150 rpm). CGRP (100 nM, GenScript) or vehicle (DMEM) were added to the cells immediately before adding the bacteria. The number of bacteria in each well was determined by serial dilution plating on TSA plates with sheep blood agar (BD Biosciences), and bacterial colonies were counted after overnight incubation at 37°C in 5% CO_2.

ELISA

Mouse macrophages ($5x10^5$ cells per well) were obtained as described in *Isolation and culture of bone marrow-derived macrophages* and co-incubated with *S. pneumoniae* or vehicle (DMEM + 10% mouse serum) for 24h (37°C, 5% CO_2). Cells were treated with CGRP (100 nM, GenScript) or vehicle (DMEM) immediately before adding the bacteria. After incubation, supernatants were collected, filtered, and stored in -80°C until ELISA was performed. The concentrations of CXCL10, CCL3, CCL2, and TNFα in the supernatants were determined using ELISA kits (R&D Systems) following manufacturer's protocols.

Magnetic-activated cell sorting (MACS) of meningeal cells

Mice were deeply anesthetized with intraperitoneal injection of tribromoethanol solution (Avertin, 500 mg/kg) and perfused transcardially with 30 mL saline solution. Samples from the meninges (cortical Dura mater) were dissected as previously described[5,6] and incubated for 30 min at 37°C in 0.5 mL of DMEM/F12 medium containing Dispase 1 U/mL (STEMCELL Technologies) and Liberase TL 0.25 mg/mL (Sigma). After incubation, cells were centrifuged 400*g* for 10 min, resuspended in 1 mL of ice-cold cell wash buffer (BioLegend), gently dissociated using a 1 mL pipette, and filtered through a 40 µm cell strainer (Flowmi, Scienceware). The resulting cell suspension was then used for MACS purification using CD45 MicroBeads (Miltenyi Biotech) or F4/80 MicroBeads UltraPure (Miltenyi Biotech) and MS MACS columns (Miltenyi Biotech) following manufacturer's directions.

Intra-cisterna magna injections

Injections into the cisterna magna were used to deliver bacteria into the subarachnoid space and to deplete meningeal macrophages. The procedure was performed as described previously[5] with small

modifications. Mice were first anesthetized with isoflurane (4%) in the induction chamber, and treated with carprofen (20 mg/kg, subcutaneous) and buprenorphine (0.1 mg/kg, subcutaneous) immediately prior the surgery. Corneas were maintained lubricated with Puralube and anesthesia by isoflurane was maintained through a nosecone during the surgery. Animals were transferred to stereotaxic frame, the skin of the head was shaved and aseptically prepared by swabbing betadine followed by ethanol (3 times each). Cranium was exposed by making a surgical anterior-posterior incision with a scalpel blade, and the subcutaneous tissue and muscles of the neck were gently separated to access the dura mater of the cisterna magna. *S. pneumoniae* (10^3 c.f.u., 5 µL), mannosylated liposomes containing clodronate (m-Clodrosome® Encapsula Nano Sciences, 5 µL), or empty mannosylated liposomes (m-Encapsome® Encapsula Nano Sciences, 5 µL) were injected into the subarachnoid space using a 30-gauge 0.5-inch needle mounted on a 25- µL Hamilton syringe. After injection, muscles were re-aligned, and the incision was closed using wound clips (Autoclip, 7mm) and tissue adhesive (Vetbond 3M). After surgery, animals were placed in a cage containing a warming pad and monitored for one hour after surgery. Additional doses of Carprofen (every 24h) and were administered for 72h post-surgery and wounds were monitored for adequate healing.

CGRP release assay from meninges explants

Mice were euthanized by CO_2 inhalation and the skullcap containing meninges was dissected and rapidly transferred to 24-well plates containing 1 mL of DMEM. The explants were incubated for 30 min at 32°C with gentle shaking (150 rpm). After incubation, the medium from the organ cultures was collected and used to determine the levels of CGRP with the CGRP EIA kit (Cayman Chemical) according to manufacturer`s instructions.

In vivo CGRP and BIBN4096 treatment

We evaluated the impact of CGRP signaling on the outcome of bacterial meningitis by treating mice with alpha-CGRP or with the CGRP antagonist BIBN4096 (Tocris). For these experiments, mice were treated with CGRP (0.1 mg/kg), BIBN4096 (0.3 mg/kg), or vehicle via intraperitoneal injection. Treatments were performed 2h prior to induction of bacterial meningitis as described in the section *Hematogenous bacterial meningitis* and again 24h later. Treatment doses were selected based on previous publications using these compounds[7,8]

Flow cytometry

Mice were deeply anesthetized with intraperitoneal injection of tribromoethanol solution (Avertin, 500 mg/kg) and perfused transcardially with 30 mL saline solution. Meninges were dissected, minced, and incubated for 30 min at 37°C in 0.5 mL of DMEM/F12 medium containing Dispase (1 U/mL, STEMCELL Technologies) and Liberase TL (0.25 mg/mL, Sigma). After incubation, cells were centrifuged at 400*g* for 10 min, resuspended in 1 mL of ice-cold cell wash buffer (BioLegend), gently dissociated using a 1 mL pipette, and filtered through a 40 µm cell strainer (Flowmi, Scienceware), The resulting cell suspension was incubated with mouse FcR Blocking Reagent (Miltenyi Biotec) for 10 min, and then incubated with the following reagents: DAPI (4',6-Diamidino-2-Phenylindole, Dilactate, 3 µM, BioLegend), anti-mouse CD45-PE-Cy7 clone 30-F11 (1:200, BioLegend), anti-mouse CD11b Brilliant Violet® 570 or APC clone M1/70 (1:200, BioLegend), anti-mouse Ly-6C Brilliant Violet® 650 clone HK1.4 (1:200, BioLegend), anti-mouse CD206 (Mrc1) PE clone C068C2 (1:200, BioLegend), anti-mouse Ly-6G PE-Cyanine5 or APC-Cyanine7 clone 1A8 (1:200, Thermo Fisher Scientific), anti-mouse CD3 FITC or Alexa Fluor 700 clone 17A2 (1:200, BioLegend), and anti-mouse CD19 PE-Cyaine5.5 clone 1D3 (1:200, Thermo Fisher Scientific). After incubation, cells were centrifuged for 5 min at 300*g* and resuspended in 500 µL of cell wash buffer, then

centrifuged again and resuspended in wash buffer containing 2% PFA. Flow cytometry was performed on a FACSymphony A5 flow cytometer (BD Biosciences). Flow cytometry data were collected and exported using BD FACSDiva software (BD Biosciences) and analyzed using FlowJo software (FlowJo LLC). A small aliquot (20 µL) was used to count the total number of cells in each sample and the results were used to convert the percentages of immune cell populations into cell numbers.

Quantitative RT-PCR

Mouse macrophages were obtained as described in *Isolation and culture of bone marrow-derived macrophages*. Macrophages ($5x10^5$ cells per well) were incubated with *S. pneumoniae* ($5x10^5$ c.f.u. per well) and CGRP (100 nM) or vehicle (DMEM) in DMEM supplemented with 10% of mouse serum for 4h (37°C, 5% CO_2). In some wells, the cells were pre-treated with the selective PKA inhibitor Rp-8-CPT-cAMP (10 µM, Cayman Chemical) 1h before incubation. After incubation, supernatant was removed and replaced by 500 µL of Trizol, and plates were frozen at −80°C until RNA extraction. For total RNA extraction, samples were thawed at room temperature, mixed with 100 µL of chloroform, and centrifuged at 12,000 g for 15 min at 4°C. The aqueous phase was collected to a new tube and combined with equal parts of isopropyl alcohol, mixed well, and centrifuged at 12,000 g for 10 min at 4°C. After discarding the supernatant, 500 µL of 75% ethanol was added to the samples, vortexed well, and centrifuged at 7,500 g for 5 min. Supernatant was then discarded and the pellet containing RNA was resuspended in 50 µL of nuclease-free water. The mRNA in the samples was reverse transcribed into cDNA using iScript cDNA Synthesis Kit (Biorad). Relative gene expression was determined using gene-specific primers (PrimerBank) and SYBR Green Master Mix (Life Technologies) on a QuantStudio 5 RT-PCR System (Applied Biosystems). Expression data was collected and exported using the QuantStudio Design & Analysis Software v1.5.1 (Applied Biosystems). Expression levels were normalized to beta-actin expression (*Actb*) using the $2^{-\Delta Ct}$

method. Primer sequences(5' to 3'): *Actb* forward: AGCTGCGTTTTACACCCTTT, *Actb* reverse AAGCCATGCCAATGTTGTCT, *Ramp1* forward: GGATGAGAGTCCCATAGTCAGG, *Ramp1* reverse GGGGCTCTGCTTGCCAT, *Jdp2* forward: CTCCTCCTGCTATGATGCCT, *Jdp2* reverse CTCTTGCCCAGTTTCACCTC, *Crem* forward: TGGACTGTGGTACGGCCAAT, *Crem* reverse CAGTTTCATCTCCAGTTACA, *Tnf* forward: CAGGCGGTGCCTATGTCTC, *Tnf* reverse CGATCACCCCGAAGTTCAGTAG, *Ccl2* forward: TTAAAAACCTGGATCGGAACCAA, *Ccl2* reverse GCATTAGCTTCAGATTTACGGGT, *Ccl3* forward: TTCTCTGTACCATGACACTCTGC, *Ccl3* reverse CGTGGAATCTTCCGGCTGTAG, *Cxcl10* forward: CCAAGTGCTGCCGTCATTTTC, *Cxcl10* reverse GGCTCGCAGGGATGATTTCAA, *Ccl7* forward: GCTGCTTTCAGCATCCAAGTG, *Ccl7* reverse CCAGGGACACCGACTACTG.

RNA-sequencing of macrophages

Macrophages were cultured as described in *Isolation and culture of bone marrow-derived macrophages*. Cells ($1x10^6$ per well) were incubated with 10% mouse serum-opsonized *S. pneumoniae* ($1x10^6$ c.f.u.) and CGRP (100 nM) or vehicle (PBS) for 4h. After incubation, supernatant was removed and replaced by 500 µL of Trizol, and plates were frozen at −80°C until RNA extraction as described in *Quantitative RT-PCR*. RNA-seq library preparation (Kapa mRNA Hyperprep, Roche) and sequencing (NovaSeq SP, 2x50bp, Illumina) was conducted by the Bauer Sequencing Core at Harvard University.

Single-cell RNA-sequencing of meninges

Samples containing meningeal immune cells (CD45-enriched) or meningeal non-immune cells (CD45-depleted) were obtained as described in *Magnetic-activated cell sorting (MACS) of meningeal cells* and

used for droplet-based single-cell RNA-sequencing (10x Genomics). Library preparation (Chromium Next GEM Single Cell 3' Reagent Kit v3.1) and sequencing (Illumina NovaSeq 6000 System) were conducted by the Bauer Sequencing Core at Harvard University following manufacturer's instructions. The quality of the single-cell suspensions (viability >80%, concentration = 1000 cells/μL) was confirmed immediately before encapsulation using acridine orange/propidium iodide stain (Logos Biosystems) and a LUNA-FX7 (Logos Biosystems). Encapsulation of cells was performed in the Chromium Controller (10x Genomics) targeting 10,000 cells per sample. Following encapsulation and mRNA barcoding, cDNA was synthesized, isolated, and amplified (11 cycles) using Single Cell 3'GEM kit (10x Genomics) and SPRIselect reagent kit (Beckman Coulter). The quality of the amplified cDNA (concentration, size, purity) was verified using High Sensitivity D5000 ScreenTape and 4200 TapeStation system (Agilent Technologies). Next, amplified cDNA was used for library construction. cDNA fragmentation, end repair, A-tailing, adaptor ligation, and sample index PCR amplification were performed using Chromium Next GEM Single Cell 3' Library Kit v3.1 reagents (10x Genomics). Post library construction QC was performed using High Sensitivity D5000 ScreenTape and 4200 TapeStation system (Agilent Technologies). Quantification was performed using the Kapa qPCR Complete Universal Kit (Roche Sequencing Solutions) and CFX96 RT-PCR detection system (Bio-Rad Laboratories). For the sequencing, CD45-positive sample libraries were pooled and equally distributed across the two lanes of an Illumina NovaSeq S1 flow cell (Read1: 28 bp, i7 index: 8 bp, Read2: 90 bp). CD45-negative library was sequenced in a single lane of an Illumina NovaSeq S4 flow cell (Read1: 28 bp, i7 index: 8 bp, Read2: 90 bp). After sequencing, QC summary report confirmed that each library contained a minimum of 10,000 cells (10,545 - 12,185) and an average sequencing depth of 50,178 reads per cell. Cell Ranger (10x Genomics) analysis pipelines were used to demultiplex raw sequencing data and to perform alignment, filtering, and counting of barcodes and UMIs. Reference mouse genome mm10 version 2020-A was used. Count matrices generated by Cell Ranger imported into R (v.4.0.3) for further analysis using Seurat package (v. 4.1.0) [9,10]. Analysis was performed using only high-quality cells that had UMI counts

between 4000 and 70000 and less than 25% of their genes corresponding to the mitochondrial genome. Samples were normalized and scaled using Seurat's *SCTransform* function followed by Principal component analysis (PCA). Clustering and visualization were performed by running Uniform Manifold Approximation and Projection (UMAP) dimensional reduction of 15 principal components for each cluster resolution of 0.3. Cell types were defined by comparing cluster marker genes with previously published single-cell RNA-sequencing datasets of mouse meninges[5,11-13]. Visualization of genes illustrating expression levels was performed using R/Seurat commands (*DoHeatmap*, *FeaturePlot*, and *DotPlot*)[9,10] and R/Nebulosa package[14].

Differential expression analysis

Differential gene expression analysis was performed in sequencing datasets using the R package DESeq2 (bulk RNA-sequencing of BMDM) or Seurat (single-cell RNA-sequencing of meninges) [9,10,15]. Genes were considered to be differentially expressed when adjusted P value was lower than 0.05. The list of differentially expressed genes (DEG) was used in pathway enrichment analysis and to create volcano plots and Venn diagrams.

Pathway enrichment analysis

Pathway enrichment on the list of differentially expressed genes was analyzed using the Database for Annotation, Visualization, and Integrated Discovery (DAVID) tool (http://david.abcc.ncifcrf.gov). Gene Ontology (GO) terms in the Biological Processes category with $P < 0.05$ were considered statistically significant. Statistically significant, non-redundant GO enriched terms were plotted.

Data Availability

Single cell RNA sequencing data and bulk RNA sequencing data generated during this study are in the process of being deposited to the NCBI GEO database. The accession numbers for these datasets will be made available to reviewers upon request and to the manuscript for readers prior to publication.

Mouse grimace scale

The mouse Grimace Scale was used to quantify spontaneous pain-like behaviors as previously described [16-18]. Animals were acclimated in clear acrylic chambers (8 x 8 x 8 cm) one day prior to baseline testing. Measurements were taken at day 0 (baseline, before injection) and 1-2 days after injection with *S. pneumoniae*, *S. agalactiae*, or vehicle. Mice were individually recorded for 10 minutes with high-definition cameras (GoPro). From these 10-minute videos, the first image with a clear view of the animal's face from every minute of the video was extracted using iMovie (Apple, Inc). The selected images were randomized, and blinded scoring was performed by investigators that were unaware of the groups and time points. As described in the original method, for each image, orbital tightening, nose bulge, cheek bulge, ear position were scored (0 "not present", 1 "moderately visible" and 2 "severely visible") and the total score for each image was averaged.

General experimental design

All *in vivo* experiments were performed in both male and female age-matched littermates. Treatment groups of mice were randomized and evenly distributed across both male and female littermates in cages. In experiments involving transgenic mice, littermates with different genotypes were cohoused for the

duration of experiments. Animal numbers were estimated based on pilot studies of *S. agalactiae* and *S. pneumoniae* infections in our lab and on published works[2,19].

Immunostaining and microscopy

Meninges dissection and wholemount immunofluorescence staining were performed as described previously with small modifications [5,6]. Mice were euthanized and intracardially perfused with 30 mL of PBS, followed by 30 mL of PBS/4% PFA. The cortical meninges were dissected and post-fixed in PBS/4% PFA solution at 4°C for 24h. Before immunostaining, samples were transferred to PBS and incubated for 24h at 4°C to remove PFA. Free-floating samples were incubated with blocking solution (PBS with 0.1% Triton X-100 and 5% donkey serum) in 24-well plates for 2h at room temperature with agitation. Blocking solution was then replaced by staining solution (PBS with 0.1% Triton X-100 and 2% donkey serum) containing the primary antibodies rabbit anti-rat CGRP (1:500, C8198 Sigma) or goat anti-mouse Mrc1 (5 µg/mL, AF2535 R&D Systems) and incubated for 24h at 4°C with agitation. Samples were washed five times with PBS to remove unbound primary antibodies and then incubated (24h at 4°C with agitation) with staining solution containing the secondary antibodies donkey anti-rabbit IgG conjugated with DyLight 488 (1:500, ab98488 Abcam) or donkey anti-goat IgG conjugated with Alexa Fluor 488 (1:500, ab150129 Abcam). In some cases, bacteria were labeled with CellTracker Red CMTPX Dye (C34552 Invitrogen) 30 min before injection into mice. For the staining of blood vessels, the primary antibody rat anti-mouse CD31 conjugated with Alexa Fluor 647 (5 µg, MEC13.3 BioLegend) was injected into mice 5 minutes before perfusion. Stained samples were washed five times with PBS and mounted in Prolong® Gold Antifade Reagent (Cell Signaling). Fluorescence imaging was performed using a Leica Stellaris 8 confocal microscope (Leica) and the LAS X software (Leica). System-optimized settings were used to acquire the full thickness

of the tissue (z-axis) and for tile-stitching (x and y-axis). Merged maximum projection images were exported.

Brain histopathology

Brain samples were collected from Nav1.8-DTA and control mice 24h after injection of *S. pneumoniae* ($3x10^7$ c.f.u in 100 µL, i.v.). Mice were deeply anesthetized with tribromoethanol solution (Avertin, 500 mg/kg, i.v.) and perfused transcardially with 30 mL saline solution followed by 10 mL of PFA 4% in saline. After dissection, brain samples were maintained in PFA 4% for 3 days at 4°C. Fixed brains were embedded in paraffin, sectioned (10 µm thick), and half of the slides were stained using hematoxylin and eosin (H&E) by the Rodent Histopathology Core at Harvard Medical School. Pictures from the brain samples were taken automatically using a Leica DMi8 microscope (sCMOS camera and 40x NA 0.85 objective) and the Thunder® software (Leica). A total of 96 pictures (12 pictures x 4 samples x 2 groups) of the brain cortex images were collected and randomized for blinded scoring. Each field was assigned a score from 0 to 3 based on neuronal morphology: grade 0 (not altered), grade 1 (no vacuolation with small numbers of pyknotic cells), grade 2 (moderate vacuolation and pyknosis), and grade 3 (extensive vacuolation, pyknosis, and tissue loss or liquefactive necrosis)[20,21]. For the analysis of caspase-3 activity, slides were deparaffinized and rehydrated prior to immunostaining. Slides were heated at 60C for 10 min, washed twice with xylene for 10 min, and incubated with a series of graded ethanol solutions (100%, 95%, 70%, 50%, and 30% in PBS) for 5 min each. Slides were incubated with blocking solution (PBS with 0.1% Triton X-100 and 5% donkey serum) for 1h at room temperature. After incubation, blocking solution was removed, and slides were incubated with staining solution (PBS with 0.1% Triton X-100 and 2% donkey serum) containing rabbit anti-human cleaved caspase-3 antibody (1:400, 9661 Cell Signaling) for 24h at 4°C. Slides were rinsed five times with PBS and incubated for 2h with staining solution containing donkey

anti-rabbit IgG conjugated with Alexa Fluor 647 (1:500, Abcam) and Hoechst 33342 DNA staining solution (1 µM, Thermo Scientific). After incubation, slides were rinsed five times with PBS and coverslip mounted with Prolong® Gold Antifade Reagent (Cell Signaling). Fluorescence imaging was performed using a Leica Stellaris 8 confocal microscope (Leica) and the LAS X software (Leica). System-optimized settings were used to acquire the full thickness of the tissue (z-axis) and for tile-stitching (x and y-axis). Merged maximum projection images were exported. Fluorescence intensity was calculated with Fiji software[22] by measuring the Integrated Density of the of cleaved caspase-3 staining in the brain. Results are expressed as fold-change of control (uninfected) brain.

Statistical analysis

Statistical analysis was performed using GraphPad Prism Software. One-way analysis of variance (ANOVA) with appropriate multiple comparisons tests was used to compare three independent groups. Two-group comparisons were made using two-tailed unpaired Student's t-test. For comparisons of multiple factors, two-way ANOVA with appropriate multiple comparisons tests was used.

Method references

1 Malley, R. *et al.* Recognition of pneumolysin by Toll-like receptor 4 confers resistance to pneumococcal infection. *Proc Natl Acad Sci U S A* **100**, 1966-1971, doi:10.1073/pnas.0435928100 (2003).

2 Mu, R. *et al.* Identification of CiaR Regulated Genes That Promote Group B Streptococcal Virulence and Interaction with Brain Endothelial Cells. *PLoS One* **11**, e0153891, doi:10.1371/journal.pone.0153891 (2016).

3 Pinho-Ribeiro, F. A. *et al.* Blocking Neuronal Signaling to Immune Cells Treats Streptococcal Invasive Infection. *Cell* **173**, 1083-1097 e1022, doi:10.1016/j.cell.2018.04.006 (2018).

4 Toda, G., Yamauchi, T., Kadowaki, T. & Ueki, K. Preparation and culture of bone marrow-derived macrophages from mice for functional analysis. *STAR Protoc* **2**, 100246, doi:10.1016/j.xpro.2020.100246 (2021).

5 Alves de Lima, K. *et al.* Meningeal gammadelta T cells regulate anxiety-like behavior via IL-17a signaling in neurons. *Nat Immunol* **21**, 1421-1429, doi:10.1038/s41590-020-0776-4 (2020).

6 Louveau, A. *et al.* Structural and functional features of central nervous system lymphatic vessels. *Nature* **523**, 337-341, doi:10.1038/nature14432 (2015).

7 Argunhan, F. *et al.* Calcitonin Gene-Related Peptide Protects Against Cardiovascular Dysfunction Independently of Nitric Oxide In Vivo. *Hypertension* **77**, 1178-1190, doi:10.1161/HYPERTENSIONAHA.120.14851 (2021).

8 Rea, B. J. *et al.* Peripherally administered calcitonin gene-related peptide induces spontaneous pain in mice: implications for migraine. *Pain* **159**, 2306-2317, doi:10.1097/j.pain.0000000000001337 (2018).

9 Hafemeister, C. & Satija, R. Normalization and variance stabilization of single-cell RNA-seq data using regularized negative binomial regression. *Genome Biol* **20**, 296, doi:10.1186/s13059-019-1874-1 (2019).

10 Hao, Y. *et al.* Integrated analysis of multimodal single-cell data. *Cell* **184**, 3573-3587 e3529, doi:10.1016/j.cell.2021.04.048 (2021).

11 Rustenhoven, J. *et al.* Functional characterization of the dural sinuses as a neuroimmune interface. *Cell* **184**, 1000-1016 e1027, doi:10.1016/j.cell.2020.12.040 (2021).

12 Van Hove, H. *et al.* A single-cell atlas of mouse brain macrophages reveals unique transcriptional identities shaped by ontogeny and tissue environment. *Nat Neurosci* **22**, 1021-1035, doi:10.1038/s41593-019-0393-4 (2019).

13 Jordao, M. J. C. *et al.* Single-cell profiling identifies myeloid cell subsets with distinct fates during neuroinflammation. *Science* **363**, doi:10.1126/science.aat7554 (2019).

14 Alquicira-Hernandez, J. & Powell, J. E. Nebulosa recovers single cell gene expression signals by kernel density estimation. *Bioinformatics*, doi:10.1093/bioinformatics/btab003 (2021).

15 Yang, N. J. *et al.* Anthrax toxins regulate pain signaling and can deliver molecular cargoes into ANTXR2(+) DRG sensory neurons. *Nat Neurosci* **25**, 168-179, doi:10.1038/s41593-021-00973-8 (2022).

16 Langford, D. J. *et al.* Coding of facial expressions of pain in the laboratory mouse. *Nat Methods* **7**, 447-449, doi:10.1038/nmeth.1455 (2010).

17 Hohlbaum, K., Corte, G. M., Humpenoder, M., Merle, R. & Thone-Reineke, C. Reliability of the Mouse Grimace Scale in C57BL/6JRj Mice. *Animals (Basel)* **10**, doi:10.3390/ani10091648 (2020).

18 Whittaker, A. L., Liu, Y. & Barker, T. H. Methods Used and Application of the Mouse Grimace Scale in Biomedical Research 10 Years on: A Scoping Review. *Animals (Basel)* **11**, doi:10.3390/ani11030673 (2021).

19 Deng, L. *et al.* The Group B Streptococcal surface antigen I/II protein, BspC, interacts with host vimentin to promote adherence to brain endothelium and inflammation during the pathogenesis of meningitis. *PLoS Pathog* **15**, e1007848, doi:10.1371/journal.ppat.1007848 (2019).

20 Ekici, M. A. *et al.* Effect of etanercept and lithium chloride on preventing secondary tissue damage in rats with experimental diffuse severe brain injury. *Eur Rev Med Pharmacol Sci* **18**, 10-27 (2014).

21 Zille, M. *et al.* Visualizing cell death in experimental focal cerebral ischemia: promises, problems, and perspectives. *J Cereb Blood Flow Metab* **32**, 213-231, doi:10.1038/jcbfm.2011.150 (2012).

22 Schindelin, J. *et al.* Fiji: an open-source platform for biological-image analysis. *Nat Methods* **9**, 676-682, doi:10.1038/nmeth.2019 (2012).

Supplementary Files

This is a list of supplementary files associated with this preprint. Click to download.

- SupplementaryFigure1.pdf